Master's Thesis

Exploring the potential of five satellite-derived soil moisture products for simulating long term irrigation datasets using the SM Delta approach

submitted in satisfaction of the requirements for the degree
Diplom-Ingenieurin
of the TU Wien, Faculty of Civil and Environmental Engineering

---

Diplomarbeit

Untersuchung von fünf satellitenbasierten Bodenfeuchteprodukten zur Langzeitmodellierung von Bewässerungsdatensätzen mittels SM Delta Methode

ausgeführt zum Zwecke der Erlangung des akademischen Grads
Diplom-Ingenieurin
eingereicht an der TU Wien, Fakultät für Bau- und Umweltingenieurwesen

Pia Langhans, BSc

Matr.Nr.: 11701227

Supervision: Univ.Prof. Dr.rer.nat. **Wouter Dorigo**, MSc
Pojektass. Dr. **Pierre Laluet**, MSc
Fakultät für Mathematik und Geoinformation
Department für Geodäsie und Geoinformation
Forschungsbereich Klima- und Umweltfernerkundung
Technische Universität Wien
Wiedner Hauptstraße 8/E120, 1040 Wien, Österreich

Wien, January 13, 2025

Die approbierte gedruckte Originalversion dieser Diplomarbeit ist an der TU Wien Bibliothek verfügbar
The approved original version of this thesis is available in print at TU Wien Bibliothek.

Die approbierte gedruckte Originalversion dieser Diplomarbeit ist an der TU Wien Bibliothek verfügbar
The approved original version of this thesis is available in print at TU Wien Bibliothek.

Declaration

I hereby declare that I have written this thesis independently, that I have completely specified the utilized sources and resources and that I have definitely marked all parts of the work - including tables, maps and figures - which belong to other works or to the internet, literally or extracted, by referencing the source as borrowed.

Wien, December 2024: _____

Pia Langhans

Die approbierte gedruckte Originalversion dieser Diplomarbeit ist an der TU Wien Bibliothek verfügbar
The approved original version of this thesis is available in print at TU Wien Bibliothek.

Die approbierte gedruckte Originalversion dieser Diplomarbeit ist an der TU Wien Bibliothek verfügbar
The approved original version of this thesis is available in print at TU Wien Bibliothek.

Acknowledgements

This thesis would not have been possible without the guidance and support of several people.

First of all, I want to thank my supervisor *Pierre Laluet* for his support and guidance throughout the process. Thank you for always answering my questions and providing detailed feedback from which I learned a lot. I am also grateful to *Prof. Wouter Dorigo* for his support and for giving me the opportunity to work on this thesis and as a student employee in the CLIMERS research group alongside my studies.

I also want to thank my colleagues in the GEO department and my fellow students from Technical Physics and Environmental Engineering who made my time at the University truly unforgettable. Thank you for being part of this journey.

A very special thank you goes to my boyfriend for his unconditional support and belief in me.

Finally, I would like to express my gratitude to my family, especially my parents, for always supporting me. Thank you for encouraging my interest in natural sciences since childhood and always believing in my abilities to achieve the goals I wanted to reach.

Thank you!
Danke!

Die approbierte gedruckte Originalversion dieser Diplomarbeit ist an der TU Wien Bibliothek verfügbar
The approved original version of this thesis is available in print at TU Wien Bibliothek.

Die approbierte gedruckte Originalversion dieser Diplomarbeit ist an der TU Wien Bibliothek verfügbar
The approved original version of this thesis is available in print at TU Wien Bibliothek.

Abstract

Irrigation accounts for approximately 70 % of global freshwater withdrawals, significantly impacting the water cycle through reduced streamflow and groundwater tables and increased evapotranspiration. Accurate long-term estimates of irrigation water use (IWU) are essential for improving climate model simulations. However, in situ irrigation data are extremely rare on a global scale, and statistical surveys, as well as irrigation simulated by models, are too uncertain to provide reliable estimates. Satellite-derived soil moisture (SM) data offer a promising alternative approach for monitoring long-term IWU globally.

This thesis builds on the Soil Moisture (SM) Delta method, which estimates IWU by calculating the differences between satellite and modeled SM data. The approach is based on the fact that satellite-based SM theoretically contains an irrigation signal, whereas model-based SM lacks such a signal if irrigation is not modeled. The methodology is used to assess the ability of five satellite-based SM products to retrieve long-term irrigation estimates. 15-year IWU datasets have been produced over the Ebro Basin (86,000 km^2) and the Murray-Darling Basin (1,000,000 km^2) using coarse-scale (0.25°) SM data, and validated against in situ IWU data from an irrigation district in the Ebro Basin and four irrigation districts in the Murray-Darling Basin.

Validation of the IWU estimates against in situ IWU data from the irrigation district in the Ebro Basin showed a significant correlation when using the ESA CCI COMBINED product (R=0.75), which also yielded the lowest Root Mean Square Deviation (RMSD=22.84 mm/month), showing the best performance over this basin. In the Murray-Darling Basin, validation results varied among the four irrigation districts, with ESA CCI ACTIVE performing best in three irrigation districts (R=0.40, RMSD=21.84, bias=4.01 mm/month on average) and ESA CCI PASSIVE in one district (R=0.64, RMSD=19.70 mm/month, bias=0.83 mm/month). In terms of overall performance, ESA CCI COMBINED proved to be the most reliable product with a good balance between low RMSD (22.01 mm/month on average) and the highest correlation (R=0.45 on average) in the four irrigation districts.

All products show an underestimation of IWU in the Ebro Basin, which could be improved by including evapotranspiration in the algorithm. Furthermore, when compared with studies obtaining high-resolution IWU estimates, our coarse-resolution method performed comparably well in the Ebro Basin. These large-scale, long-term IWU datasets are an important step towards better accounting for the impacts of irrigation in climatic and hydrological modeling and can improve water resource management.

Die approbierte gedruckte Originalversion dieser Diplomarbeit ist an der TU Wien Bibliothek verfügbar
The approved original version of this thesis is available in print at TU Wien Bibliothek.
TU Bibliothek Your knowledge hub WIEN

Die approbierte gedruckte Originalversion dieser Diplomarbeit ist an der TU Wien Bibliothek verfügbar
The approved original version of this thesis is available in print at TU Wien Bibliothek.

Kurzfassung

Die Bewässerung macht etwa 70 % der globalen Süßwasserentnahmen aus und beeinflusst den Wasserkreislauf erheblich durch erhöhten Wasserverbrauch und Evapotranspiration. Präzise langfristige Schätzungen des Wasserverbrauchs durch Bewässerung sind entscheidend für die Verbesserung von Klimamodellen. In situ Messungen bieten jedoch keine globale Abdeckung, und modellierte Bewässerungsdaten sind zu ungenau, um verlässliche Schätzungen zu liefern, wodurch leistungsfähigere Methoden erforderlich werden. Satellitenbasierte Bodenfeuchtedaten bieten eine vielversprechende alternative Möglichkeit zur Überwachung des langfristigen Wasserverbrauchs durch Bewässerung auf globaler Ebene.

Diese Arbeit baut auf der SM-Delta-Methode auf, welche den Wasserverbrauch durch Bewässerung abschätzt, indem sie Unterschiede zwischen satellitenbasierten und modellierten Bodenfeuchtedaten berechnet. Die Methode wird verwendet, um die Fähigkeit von fünf satellitengestützten Bodenfeuchteprodukten zu bewerten langfristige Bewässerungsschätzungen zu erhalten. 15-jährige Bewässerungsdatensätze wurden über dem Ebro-Becken (86.000 km²) und dem Murray-Darling-Becken (1.000.000 km²) unter Verwendung von grob aufgelösten (0,25°) Bodenfeuchtedaten erstellt und anhand von in situ Bodenfeuchtedaten aus einem Bewässerungsgebiet im Ebro-Becken und vier im Murray-Darling-Becken validiert.

Die Validierung gegenüber in situ Bewässerungsdaten im Ebro-Becken zeigte eine starke Korrelation für das ESA CCI COMBINED Produkt (R=0,75), das zudem die niedrigste Root Mean Square Deviation (RMSD=22,84 mm/Monat) aufwies und somit das geeignetste Produkt für diese Region darstellt. Im Murray-Darling-Becken variierten die Validierungsergebnisse zwischen den vier Bewässerungsgebieten, wobei ESA CCI ACTIVE in drei Bewässerungsgebieten am besten abschnitt (R=0,40, RMSD=21,84 mm/Monat, bias=4,01 mm/Monat im Durchschnitt) und ESA CCI PASSIVE in einem Gebiet (R=0,64, RMSD=19,70 mm/Monat, bias=0,83 mm/Monat). In Bezug auf die Gesamtleistung erwies sich ESA CCI COMBINED als das zuverlässigste Produkt mit einem guten Gleichgewicht zwischen niedrigem RMSD (22,01 mm/Monat im Durchschnitt) und starker Korrelation (R=0,45 im Durchschnitt) in den vier Bewässerungsgebieten.

Alle Produkte zeigen eine Unterschätzung der Bewässerung im Ebro-Einzugsgebiet, die durch die Einbeziehung der Evapotranspiration in den Algorithmus verbessert werden könnte. Im Vergleich zu Studien, in denen Bewässerungsschätzungen mit hoher Auflösung vorgenommen wurden, schnitt unsere grob aufgelöste Methode im Ebro-Becken vergleichbar gut ab. Diese groß angelegten, langfristigen Bewässerungsdatensätze sind ein wichtiger Schritt zur besseren Berücksichtigung der Auswirkungen der Bewässerung in klimatischen und hydrologischen Modellen und können das Management der Wasserressourcen verbessern.

Die approbierte gedruckte Originalversion dieser Diplomarbeit ist an der TU Wien Bibliothek verfügbar
The approved original version of this thesis is available in print at TU Wien Bibliothek.
TU Bibliothek Your knowledge hub WIEN

Die approbierte gedruckte Originalversion dieser Diplomarbeit ist an der TU Wien Bibliothek verfügbar
The approved original version of this thesis is available in print at TU Wien Bibliothek.

Contents

Die approbierte gedruckte Originalversion dieser Diplomarbeit ist an der TU Wien Bibliothek verfügbar
The approved original version of this thesis is available in print at TU Wien Bibliothek.
TU Wien Bibliothek Your knowledge hub

Die approbierte gedruckte Originalversion dieser Diplomarbeit ist an der TU Wien Bibliothek verfügbar
The approved original version of this thesis is available in print at TU Wien Bibliothek.

Introduction 1

1.1 Irrigation and climate modeling

Insufficient water availability often leads to crop yield losses, making irrigation crucial for preventing these and enhancing food security, especially in semi-arid regions [1]. Due to climate change long dry periods and water scarcity are expected to become even more severe in the future making irrigation more and more important for food security [2]. Moreover, worldwide, 20 % of cropland is irrigated while delivering 40 % of the entire food production and causing 70 % of freshwater withdrawals [3]. In addition, irrigation significantly affects the environment by causing groundwater depletion, nutrient leaching, and increasing soil salinity [4–6]. Furthermore, extensive irrigation impacts local meteorological conditions by increasing soil moisture (SM), which in turn elevates evapotranspiration (ET). This rise in ET has a cooling effect on surface temperatures while simultaneously enhancing humidity, cloud cover, and precipitation [7]. Additionally, irrigation influences hydroclimatic patterns both locally and remotely [8]. However, even if irrigation impacts the climate regionally, many meteorological and climate models do not directly incorporate irrigation information due to i) lack of available irrigation data (or too uncertain data), ii) too uncertain irrigation models [9]. Therefore, obtaining accurate, long-term, and global estimates of IWU is essential to ensure robust climate simulation in irrigated areas [8].

1.2 How can we obtain information on irrigation?

1.2.1 In situ irrigation and FAO statistics

Survey-based irrigation estimates are typically available only at a local scale with low temporal resolution, often limited to annual data. These estimates carry significant uncertainties due to the self-reporting of farmers, upscaling procedures, and the representativeness of surveyed farms, making them unsuitable for accurately indicating the timing and amount of individual irrigation events [10]. The Food and Agriculture Organization (FAO) of the United Nations provides country-level data on irrigation water withdrawals worldwide [11]. Although these surveys are essential for validating estimated IWU, they lack the spatial and temporal detail needed for integration into climate models, where fine-scale irrigation dynamics are crucial for accurate predictions.

[1]: Kukal et al. (2019), 'Irrigation-limited yield gaps: trends and variability in the United States post-1950'

[2]: Allan et al. (2008), 'Atmospheric warming and the amplification of precipitation extremes.'

[3]: WWAP (UNESCO World Water Assessment Programme) (2019), *The United Nations world water development report 2019: leaving non one behind*

[4]: Deng et al. (2018), 'Changes in Irrigation Practices Likely Mitigate Nitrous Oxide Emissions From California Cropland'

[5]: Famiglietti (2014), 'The global groundwater crisis'

[6]: Pokhrel et al. (2016), 'Recent progresses in incorporating human land–water management into global land surface models toward their integration into Earth system models'

[7]: Cook et al. (2015), 'Irrigation as an historical climate forcing.'

[8]: McDermid et al. (2023), 'Irrigation in the Earth system'

[9]: Puy et al. (2022), 'The delusive accuracy of global irrigation water withdrawal estimates'

[10]: Massari et al. (2021), 'A Review of Irrigation Information Retrievals from Space and Their Utility for Users'

[11]: FAO (2021), *AQUASTAT - FAO's Global Information System on Water and Agriculture*

Die approbierte gedruckte Originalversion dieser Diplomarbeit ist an der TU Wien Bibliothek verfügbar
The approved original version of this thesis is available in print at TU Wien Bibliothek.
TU Bibliothek Your knowledge hub WIEN

1.2.2 Modeling

Hydrological models quantify irrigation water withdrawals and could represent an alternative to survey-based irrigation estimates. Puy et al. (2022) [9] analyzed the accuracy of global irrigation water withdrawal estimates. Models use an empirically and arbitrarily defined SM threshold to trigger irrigation, not reflecting agricultural practices [12]. In addition, irrigation efficiency, the ratio of water used by crops to the total water taken from the source, is also often uncertain and differs between irrigation districts [9], making models even more uncertain.

[12]: Olivera-Guerra et al. (2023), 'Modeling actual water use under different irrigation regimes at district scale: Application to the FAO-56 dual crop coefficient method'

1.2.3 Remote sensing

Remote sensing allows for consistently measuring land surface conditions, including those related to irrigation practices, at global scale, fine resolution, and long periods. As our method is based on the use of remote sensing-derived SM, this subsection aims to provide the theoretical background necessary to understand what these SM products are, and how they are obtained.

Remote sensing measures and analyzes electromagnetic waves emitted or reflected by an object to observe information about its properties [13]. Various wavelengths of the electromagnetic spectrum are used for remote sensing. The electromagnetic spectrum spans from a wavelength of 10^{-16} m to 10^{8} m or, expressed in frequency, from 1 Hz to 10^{24} Hz. The spectrum is divided into the following regions: gamma rays (highest frequency and shortest wavelength), X-rays, ultraviolet, visible light, infrared, microwaves, and radio waves (lowest frequency and longest wavelength) [14]. Various useful data for tracking agricultural water flows can be derived from electromagnetic waves captured by satellites using specific algorithms. Thermal infrared observations are used to estimate surface temperature, visible, near-, and shortwave-infrared bands reveal vegetation growth stages, and microwave data provides information on SM [13].

[13]: Elachi et al. (2021), *Introduction to the physics and techniques of remote sensing*

[14]: Demtröder (2017), *Experimentalphysik 2*

Microwaves are highly sensitive to the soil's dielectric properties correlated with the water content, which enables microwave sensing to estimate SM [15]. Microwave remote sensing employs both active and passive sensors, operating at a wavelength spectrum between 1 mm and 1 m, which is divided into several bands. The most commonly used bands are presented in Table 1.1 [16]. Passive sensors, which are called microwave radiometers, measure microwaves naturally emitted by the Earth's surface which are non-coherent, whereas active sensors emit microwaves and measure the backscattered signal. For active sensors, a further distinction between scatterometers, side-looking radars, and radar-altimeters is made. To measure SM, both scatterometers and microwave radiometers are used [17].

[15]: Schmugge (1987), 'Remote sensing applications in hydrology'

[16]: Lusch (1999), *Introduction To Microwave Remote Sensing*

[17]: Das et al. (2015), 'Present status of soil moisture estimation by microwave remote sensing'

A major advantage of microwaves is their independence from the weather, due to their high transmissivity through the atmosphere. In addition, microwave remote sensing systems are independent of sunlight, allowing them to operate 24 hours a day [13]. The penetration depth of microwaves is significantly larger compared to optical wavelengths. Depending on the wavelength, the measurement angle, and the SM, the signal can

[13]: Elachi et al. (2021), *Introduction to the physics and techniques of remote sensing*

Die approbierte gedruckte Originalversion dieser Diplomarbeit ist an der TU Wien Bibliothek verfügbar
The approved original version of this thesis is available in print at TU Wien Bibliothek.
TU Bibliothek Your knowledge hub WIEN

band	wavelength	frequency
L	30-15 cm	1-2 GHz
C	7.5-3.75 cm	4-8 GHz
X	3.75-2.5 cm	8-12 GHz
Ku	2.5-1.6 cm	12-18 GHz

Table 1.1: Commonly used bands in microwave remote-sensing [16].

penetrate up to one meter or more into the surface [13]. Observations in the L-band for example show a better capacity to penetrate vegetation and sense soil to a greater depth compared to the C-band or X-band. In return, suitable spatial resolution (0.25°) is more difficult to achieve with the L-band compared to the C- and X-band [18].

[18]: Dorigo et al. (2017), 'ESA CCI Soil Moisture for improved Earth system understanding: State-of-the art and future directions'

Assimilation

One approach is to assimilate variables related to irrigation observed by satellites, such as backscatter, brightness temperature, or SM to adjust model variables to each observation by adding more or less irrigation [19]. However, assimilation techniques to retrieve irrigation still need further efforts in terms of modeling and data integration [20, 21].

[19]: De Lannoy et al. (2022), 'Perspective on satellite-based land data assimilation to estimate water cycle components in an era of advanced data availability and model sophistication'

[20]: Kumar et al. (2015), 'Evaluating the utility of satellite soil moisture retrievals over irrigated areas and the ability of land data assimilation methods to correct for unmodeled processes'

[21]: Modanesi et al. (2022), 'Challenges and benefits of quantifying irrigation through the assimilation of Sentinel-1 backscatter observations into Noah-MP'

Satellite-based irrigation retrieval

Satellite observations of hydrological variables—such as SM, ET, vegetation growth, and Land Surface Temperature (LST)—provide valuable proxies for irrigation. Remote sensing offers comprehensive and consistent monitoring of the Earth's surface, delivering spatially detailed and temporally frequent data that can help improve our understanding of irrigation dynamics [10].

[10]: Massari et al. (2021), 'A Review of Irrigation Information Retrievals from Space and Their Utility for Users'

Several studies have used ET data to estimate IWU. Van Eekelen et al. (2015) [22] introduced an approach that combines land use, rainfall, and evaporation data to spatially estimate water withdrawals. More recently, Brombacher et al. (2022) [23] utilized high-resolution ET to compare irrigated and non-irrigated pixels to derive monthly IWU over the Ebro Basin in Spain. However, their analysis was limited to a single year, making it insufficient for long-term climate studies where extended temporal coverage is critical.

[22]: van Eekelen et al. (2015), 'A novel approach to estimate direct and indirect water withdrawals from satellite measurements: A case study from the Incomati basin'

[23]: Brombacher et al. (2022), 'A novel evapotranspiration based irrigation quantification method using the hydrological similar pixels algorithm'

LST has also been explored for irrigation detection. Olivera-Guerra et al. (2020) [24] applied Landsat optical and thermal data to estimate irrigation amounts in several wheat fields in central Morocco, showcasing LST's potential in monitoring irrigation.

[24]: Olivera-Guerra et al. (2020), 'Irrigation retrieval from Landsat optical/thermal data integrated into a crop water balance model: A case study over winter wheat fields in a semi-arid region'

SM data has proven particularly promising for irrigation detection, with approaches such as the SM Delta [25–28] and SM Inversion [29–33] techniques extensively studied. The SM Inversion method estimates irrigation using the soil water balance equation [1], calculating irrigation as the residual after subtracting precipitation from total soil water input. Both coarse and high-resolution SM satellite products have already been used in studies based on the SM Inversion approach [29–33].

1: $Z \cdot dS(t)/dt = i(t) + r(t) - g(t) - sr(t) - e(t)$, where Z [mm] is the water capacity, S(t) [-] is the relative SM, t [d] is the time, i(t) [mm/d] is the irrigation rate, r(t) [mm/d] is the rainfall rate, g(t) [mm/d] is the drainage term, sr(t) [mm/d] is the surface runoff and e(t) [mm/d] is the ET rate

The SM Delta method calculates irrigation as the difference between observed and modeled SM variations. It takes advantage of the fact,

Die approbierte gedruckte Originalversion dieser Diplomarbeit ist an der TU Wien Bibliothek verfügbar
The approved original version of this thesis is available in print at TU Wien Bibliothek.
TU Bibliothek Your knowledge hub WIEN

that satellite-derived SM contains an irrigation signal, whereas modeled SM does not. Hence, IWU can be derived by computing the difference between satellite and modeled SM variations. The SM Delta method has been applied across different regions with varying resolutions and time frames. The following section highlights key studies that have applied the SM Delta method.

1.2.4 SM Delta approach: State of the art

Kumar et al. (2015) [20] first studied the applicability of satellite-derived SM for irrigation retrieval. They showed that it is possible to map irrigated areas based on satellite SM.

Zaussinger et al. (2019) [25] developed the SM Delta method, which defines an irrigation event as a simultaneous increase in satellite SM and a decrease in model SM. The irrigation amount for each event is calculated as the difference between satellite SM and model SM over two time steps. Seasonal IWU is then defined as the accumulated irrigation from the start to the end of the growing season. In their study, Zaussinger et al. (2019) first computed the correlations of three satellite sensors (Soil Moisture Active Passive (SMAP), Advanced Microwave Scanning Radiometer 2 (AMSR2), and Advanced Scatterometer (ASCAT)) against a modeled SM product (Modern-Era Retrospective Reanalysis for Research and Application 2 (MERRA-2)) and found that correlations are lower over irrigated areas compared to non-irrigated areas indicating the potential of satellite SM to detect irrigation. Then, they retrieved IWU from the aggregated difference between satellite and model SM variations over the Contiguous United States (CONUS) from 2013-2016. Validation of IWU against state-aggregated observed and reported irrigation volumes showed the highest correlation for the SMAP-derived IWU (R=0.80), followed by AMSR-2 (R=0.56) and ASCAT (R=0.36). However, the obtained bias values indicate a significant underestimation for the three products ($bias_{SMAP}$ = -2.47 km^3, $bias_{AMSR-2}$ = -2.32 km^3, and $bias_{ASCAT}$ = -2.29 km^3). They point out that a limitation of the coarse-resolution satellite SM products is that the area of irrigated fields is much smaller than the area covered by a pixel, so the algorithm fails to capture local irrigation patterns.

Zohaib et Choi (2020) [34] analyzed IWU estimated from satellite and reanalysis SM globally from 2000 to 2015. They revealed that the Kolmogorov-Smirnov (KS) metric between the three ESA CCI SM products and ERA5 SM significantly differs between irrigated and non-irrigated areas, indicating the potential of satellite-derived SM to retrieve irrigation. Validation against country-level IWU from FAO showed a high correlation (R $\approx$ 0.80) and high negative biases (-76.55 km^3, -76.01 km^3 and 73.93 km^3 for the ACTIVE, PASSIVE and COMBINED product, respectively). However, as already present in Zaussinger et al. (2019) [25], IWU amounts were systematically underestimated.

Zappa et al. (2021) [26] introduced a method to use RT1 Sentinel-1 SM [35] for irrigation retrieval at 500 m sampling. Furthermore, they improved irrigation estimates by implementing an ET and a drainage term in the formulation. They showed that the contribution of ET to the irrigation estimates was twice as high as the contribution of SM.

[29]: Brocca et al. (2015), 'Rainfall estimation from in situ soil moisture observations at several sites in Europe: an evaluation of the SM2RAIN algorithm'
[30]: Dari et al. (2023), 'Regional data sets of high-resolution (1 and 6 km) irrigation estimates from space'
[31]: Dari et al. (2022), 'Irrigation estimates from space: Implementation of different approaches to model the evapotranspiration contribution within a soil-moisture-based inversion algorithm'
[32]: Dari et al. (2020), 'Exploiting High-Resolution Remote Sensing Soil Moisture to Estimate Irrigation Water Amounts over a Mediterranean Region'
[33]: Jalilvand et al. (2019), 'Quantification of irrigation water using remote sensing of soil moisture in a semi-arid region'
[20]: Kumar et al. (2015), 'Evaluating the utility of satellite soil moisture retrievals over irrigated areas and the ability of land data assimilation methods to correct for unmodeled processes'
[25]: Zaussinger et al. (2019), 'Estimating irrigation water use over the contiguous United States by combining satellite and reanalysis soil moisture data'
[34]: Zohaib et al. (2020), 'Satellite-based global-scale irrigation water use and its contemporary trends'
[26]: Zappa et al. (2021), 'Detection and Quantification of Irrigation Water Amounts at 500 m Using Sentinel-1 Surface Soil Moisture'
[35]: Quast et al. (2019), 'A Generic First-Order Radiative Transfer Modelling Approach for the Inversion of Soil and Vegetation Parameters from Scatterometer Observations'

Die approbierte gedruckte Originalversion dieser Diplomarbeit ist an der TU Wien Bibliothek verfügbar
The approved original version of this thesis is available in print at TU Wien Bibliothek.
TU Bibliothek Your knowledge hub WIEN

In another study, Zappa et al. (2022) [27] investigated the influence of SM spatio-temporal resolution on the detection of individual irrigation events by introducing a synthetic experiment. By varying the frequency and spatial resolution of the SM data used in the SM Delta algorithm, they found that IWU becomes increasingly underestimated with sampling intervals greater than one day. This underestimation also scales with the irrigated fraction of the pixel, indicating that coarser spatial resolution tends to produce larger underestimations.

[27]: Zappa et al. (2022), 'How accurately can we retrieve irrigation timing and water amounts from (satellite) soil moisture?'

In their most recent study, Zappa et al. (2024) [28] compared irrigation retrieval from two satellite-based methods, SM Delta and SM Inversion, using high-resolution Sentinel-1-derived SM data (1 km), and from a land surface model, Noah-MP. They found that SM Delta and SM Inversion can distinguish irrigated from non-irrigated areas fairly well and show much better performance (R ≈ 0.7, bias ≈ -4 mm/15 days, ubRMSD ≈ 12 mm/15 days) than NOAH-MP (R ≈ 0.7, bias ≈ 18 mm/15 days, ubRMSD ≈ 29 mm/15 days) in the Ebro Basin.

[28]: Zappa et al. (2024), 'Benefits and pitfalls of irrigation timing and water amounts derived from satellite soil moisture'

To date, most studies have primarily focused on short investigation periods, with only limited exploration of different regions, highlighting the need for more comprehensive, long-term analyses.

1.3 Objective

The objective of this thesis is to investigate the potential of five coarse-resolution satellite-derived SM products for long-term irrigation simulation, using the SM Delta method to estimate irrigation. This method is applied to two distinct regions: the Ebro Basin in Spain and the Murray-Darling Basin in Australia. Additionally, the simulated irrigation datasets are compared with benchmark irrigation data available for districts within these basins, enabling an assessment of agreement between simulated and in situ IWU.

The overarching goal is to develop a methodology for accurately simulating IWU at a coarse spatial resolution over long-term periods. Additionally, the following research questions are addressed:

Research Questions

- Which satellite-derived SM product is most suitable for developing a coarse-scale, long-term irrigation dataset based on key statistical metrics (KS-value, bias, RMSD, and Pearson correlation) computed against modeled SM? How do these metrics vary between irrigated and non-irrigated seasons for different SM products?
- What is the frequency of satellite SM observations in the study areas, and how does this frequency differ across various satellite products?
- Which satellite-derived SM product is most suitable for accurately estimating long-term global IWU, based on bias, correlation, and RMSD, when compared to in situ observations?

Die approbierte gedruckte Originalversion dieser Diplomarbeit ist an der TU Wien Bibliothek verfügbar
The approved original version of this thesis is available in print at TU Wien Bibliothek.
TU Bibliothek Your knowledge hub WIEN

1.4 Thesis Outline

Chapter 2 gives an overview of the study areas and the datasets used. In Chapter 3 the SM Delta approach is described, followed by the preprocessing of the datasets and the statistical metrics used. The results are presented in Chapter 4 and later discussed in Chapter 5. A conclusion is given in Chapter 6.

Die approbierte gedruckte Originalversion dieser Diplomarbeit ist an der TU Wien Bibliothek verfügbar
The approved original version of this thesis is available in print at TU Wien Bibliothek.
TU Bibliothek Your knowledge hub WIEN

Material 2

The objective of this section is to provide an overview of the analyzed study areas and the employed data. Firstly, the two study areas are presented in Section 2.1, namely the Ebro Basin and the Murray-Darling Basin. Then, in Section 2.2, the SM datasets, categorized into modeled and satellite-based SM, are introduced. Finally, ancillary data is presented, namely in situ data for the Ebro Basin and the Murray-Darling Basin in Section 2.2.2, as well as ESA CCI landcover maps used for masking non-irrigated areas in Section 2.2.3.

2.1 Study areas

2.1.1 Ebro Basin

The Ebro River Basin (~ 86 000 km²), located in Spain (Figure 2.1), is an agricultural area highly irrigated and mainly characterized by a cold semi-arid climate by the Köppen-Geiger climate classification [30, 36]. Mean annual precipitation amounts vary between 1800 mm in the Pyrenees and less than 500 mm in the agricultural valley [30]. Furthermore, ET is around 700 mm/year on average in the Ebro Basin [37] but reaches values of above 1000 mm/year in some irrigated areas, such as the Algerri-Balaguer district [38]. An extensive network of canals, dams, and reservoirs was constructed to redistribute water spatially, from the wetter mountainous regions upstream to the dryer central valley, where agricultural irrigation is applied on an area of approximately 9660 km^2, and temporally, from the wetter winter months to the dry summer months [37]. The majority of cultivated crops in the Ebro Basin are winter cereals, primarily barley and wheat (grown from March to July), and summer cereals (grown from June to October), predominantly maize. Furthermore, alfalfa and fruit trees are cultivated [38]. The Ebro Basin employs a mix of irrigation methods, including sprinkler, drip, and flood irrigation. Some regions utilize modern and efficient techniques like sprinkler and drip irrigation, while others rely on older, less efficient methods such as flood irrigation. [32]

[30]: Dari et al. (2023), 'Regional data sets of high-resolution (1 and 6 km) irrigation estimates from space'

[36]: Beck et al. (2018), 'Present and future Köppen-Geiger climate classification maps at 1-km resolution'

[37]: Bovolo et al. (2011), 'Climate Change, Water Resources and Pollution in the Ebro Basin: Towards an Integrated Approach'

[38]: Laluet et al. (2024), 'Retrieving the irrigation actually applied at district scale: Assimilating high-resolution Sentinel-1-derived soil moisture data into a FAO-56-based model'

[32]: Dari et al. (2020), 'Exploiting High-Resolution Remote Sensing Soil Moisture to Estimate Irrigation Water Amounts over a Mediterranean Region'

2.1.2 Murray-Darling Basin

The Murray-Darling Basin spans roughly 14 % of Australia (Figure 2.2), covering approximately 1,000,000 km² [30]. Classified as a dry, semi-arid region by the Köppen-Geiger climate classification [36], it is often referred to as Australia's food bowl. Its extensive water storage capacities support the majority of the nation's IWU [30].

Precipitation within the basin varies significantly, from approximately 350 mm annually in the arid western plains to 1500 mm/year in the wet, mountainous east [39]. Managed under the Murray-Darling Basin Plan, the interconnected river system is regulated by sustainable diversion

[30]: Dari et al. (2023), 'Regional data sets of high-resolution (1 and 6 km) irrigation estimates from space'

[36]: Beck et al. (2018), 'Present and future Köppen-Geiger climate classification maps at 1-km resolution'

[39]: Murray-Darling Basin Authority (2023), *Climate and river health*

Die approbierte gedruckte Originalversion dieser Diplomarbeit ist an der TU Wien Bibliothek verfügbar
The approved original version of this thesis is available in print at TU Wien Bibliothek.
TU Bibliothek Your knowledge hub WIEN

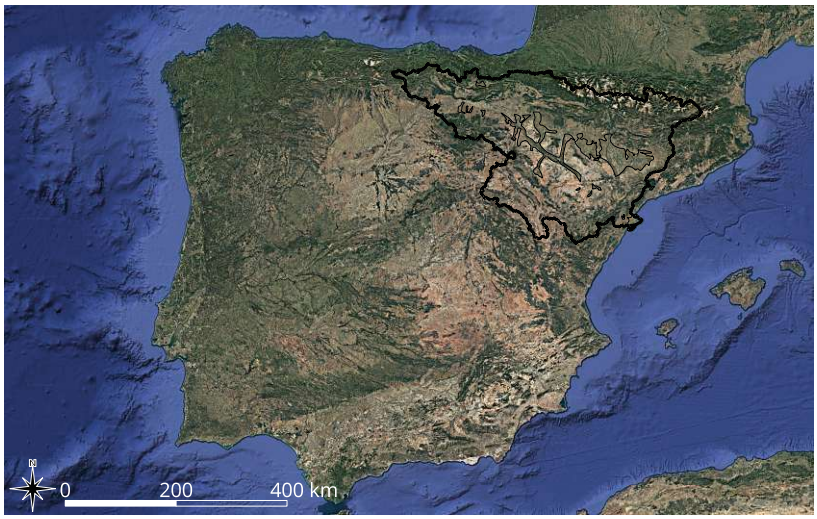

Figure 2.1: The Iberian Peninsula with the Ebro Basin (fat black line) and the irrigated areas (thin black lines). Base map from Google satellite.

limits. [40]. The basin's diverse agricultural output includes rice, maize, wheat, grapes, citrus fruits, winter and summer cereals, cotton, and pasture, with irrigation playing a critical role in sustaining productivity in its predominantly dry landscape.

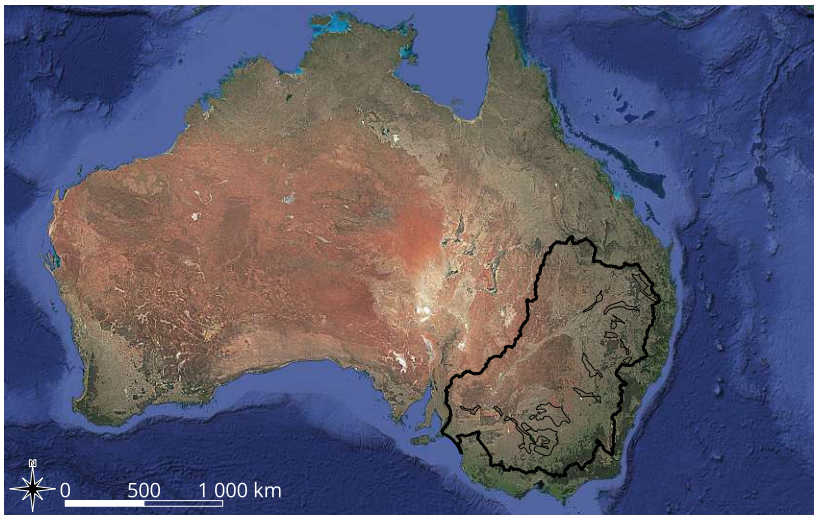

Figure 2.2: Australia with the Murray-Darling Basin (fat black line) and the irrigated areas (thin black lines). Base map from Google Satellite.

2.2 Data

2.2.1 Soil moisture data

Since the SM Delta method relies on the premise that satellite-based SM includes irrigation signals, while modeled SM does not, we first introduce the satellite and modeled SM datasets used in this study.

Die approbierte gedruckte Originalversion dieser Diplomarbeit ist an der TU Wien Bibliothek verfügbar
The approved original version of this thesis is available in print at TU Wien Bibliothek.
TU Bibliothek Your knowledge hub WIEN

Table 2.1: Time coverage, spatial resolution, revisit time, operation mode and band for the five satellite products.

satellite	time coverage	spatial res.	revisit time	active/passive	frequency
ESA CCI ACTIVE	1991/08 - onwards	0.25°	daily	active	C-band (5.3 GHz)
ESA CCI PASSIVE	1978/11 - onwards	0.25°	daily	passive	Ku-, X-, C- & L-band
ESA CCI COMBINED	1978/11 - onwards	0.25°	daily	active & passive	(1.4 - 19.3 GHz)
SMOS L2	2009/11 - onwards	42 km	3 days	passive	L-band (1.4 GHz)
SMAP L2	2015/02 - onwards	40 km	3 days	passive	L-band (1.4 GHz)

Satellite soil moisture

A variety of global SM satellite products are available. Some employ active sensors that exploit the linear relationship between backscatter and SM, while others utilize passive microwave sensors that measure microwaves emitted by the Earth [13]. Additionally, these products exhibit variability in terms of spatial and temporal resolution, and temporal coverage. Furthermore, differences in penetration depth, which depends on the band used for observation, result in varying sensitivities to vegetation. Table 2.1 presents an overview of the various satellite products used in this study.

[13]: Elachi et al. (2021), *Introduction to the physics and techniques of remote sensing*

ESA CCI SM

The European Space Agency Climate Change Initiative for soil moisture (ESA CCI SM) merges SM data retrievals from various satellites to a 0.25° grid, globally and daily aiming to retrieve an SM Climate Data Record of at least 30 years to fit to climate research needs. The product specifications are described by Dorigo et al. (2017) [18] and (2023) [41]. In the first step, Level 2 SM products are mapped to a common daily time step using the nearest neighbor search in time. Then, cumulative distribution function (CDF) matching is used to calibrate the various SM products. The merging is executed for the PASSIVE and ACTIVE products separately using Advanced Microwave Scanning Radiometer - Earth Observing System sensor (AMSR-E) and Advanced Scatterometer (ASCAT) as a reference, respectively. Furthermore, to obtain the ESA CCI COMBINED version 09.1 SM product, the ESA CCI ACTIVE and the ESA CCI PASSIVE products are first rescaled pixel-wise against the long-term Land Surface Model based SM (GLDSAS-Noah v2.1 [42]) using mean-standard deviation rescaling and are then merged. [43]

[18]: Dorigo et al. (2017), 'ESA CCI Soil Moisture for improved Earth system understanding: State-of-the art and future directions'

[41]: Dorigo et al. (2023), *ESA Climate Change Initiative Plus - Soil Moisture Algorithm Theoretical Baseline Document (ATBD) Supporting Product Version 08.1*

[42]: Rodell et al. (2004), 'The Global Land Data Assimilation System'

[43]: Dorigo et al. (2024), *ESA Climate Change Initiative Plus - Soil Moisture Algorithm Theoretical Baseline Document (ATBD) Supporting Product Version 09.0*

A triple collocation analysis (TCA) is conducted on both the ESA CCI ACTIVE and ESA CCI PASSIVE products with the objective of estimating the random error, which serves as a direct measure of the observation's sensitivity to SM changes. These random errors are used to estimate the merging parameters. The ESA CCI ACTIVE and ESA CCI PASSIVE SM products are provided with these errors at the pixel level. A TCA can only be performed if three SM products with independent error structures are available. At the global scale, this constraint can only be satisfied through the use of a combination of active and passive remotely sensed SM products and an LSM-based SM product. Therefore, a TCA is not feasible for the combined product, and classical error propagation is employed instead. [18, 44, 45]

[18]: Dorigo et al. (2017), 'ESA CCI Soil Moisture for improved Earth system understanding: State-of-the art and future directions'

[44]: Gruber et al. (2016), 'Recent advances in (soil moisture) triple collocation analysis'

[45]: Gruber et al. (2019), 'Evolution of the ESA CCI Soil Moisture climate data records and their underlying merging methodology'

The three products ESA CCI ACTIVE, ESA CCI PASSIVE, and ESA CCI COMBINED are explained in more detail in the following part:

Die approbierte gedruckte Originalversion dieser Diplomarbeit ist an der TU Wien Bibliothek verfügbar
The approved original version of this thesis is available in print at TU Wien Bibliothek.
TU Bibliothek Your knowledge hub WIEN

- The **ESA CCI ACTIVE** product merges SM products from active-microwave-based sensors, which retrieve SM using the TU Wien Water Retrieval Package (WARP) [46, 47], which is based on the linear relationship between backscatter and SM. ESA CCI SM ACTIVE uses SM data retrieved from two sensors: the European Remote Sensing (ERS) scatterometer and the Advanced Scatterometer (ASCAT). ASCAT provides SM data with an original spatial resolution of 25 km, available from May 2007. The backscatter instrument is installed on ESA's European Organisation for the Exploitation of Meteorological Satellites (EUMETSAT) meteorological operational satellites MetOp-A, which was launched in 2006, MetOp-B, launched in 2012, and MetOp-C, launched in 2018. ASCAT operates in the C-band at a frequency of 5.255 GHz and is therefore unaffected by cloud cover. The ASCAT SM product, which estimates the water content of the topsoil layer (0-5 cm) in terms of degrees of saturation (%), is based on the linear relationship between scatterometer backscatter and SM. Change detection is also used to remove contributions from vegetation, land cover, and surface topography. Satellite products operating in the C-band result in reduced penetration in the soil and higher sensitivity to vegetation compared to satellite products operating in the L-band.
- The **ESA CCI PASSIVE** product merges 12 passive microwave sensors, each with different radiometric characteristics. SM is derived from level 1 brightness temperature using the Land Parameter Retrieval Model (LPRM) [48]. Based on a microwave radiative transfer model linking SM to the observed brightness temperature, the model retrieves vegetation optical depth (VOD), SM, and surface temperature. Notably, the LPRM utilizes globally constant parameters, allowing it to compensate for variations in frequency and incidence angle across different satellite platforms. This attribute ensures the ESA CCI SM product maintains long-term consistency in SM measurements [41]. The ESA CCI PASSIVE SM product is obtained from the merging of the following passive microwave sensors (the platform is mentioned in parenthesis): SMMR (Nimbus 7), SSM/I, SSMIS (DMSP), TMI (TRMM), AMSR-E (Aqua), AMSR2 (GCOM-W1), Windsat (Coriolis), MIRAS (SMOS), SMAP (SMAP), GMI (GPM), MWRI (FY-3B, FY-3C, FY-3D).
- **ESA CCI SM COMBINED** merges the ESA CCI ACTIVE and ESA CCI PASSIVE products by rescaling the data sets against GLDAS-Noah v2.1 [42]. The merge is performed based on the weighted average between the satellite products. The weights are determined by the inverse signal-to-noise ratio. In addition, breaks that occur as a result of merging different products are detected and corrected using Quantile Category Matching (QCM) with ERA5-SM as the reference. [41] Errors of the ESA CCI SM COMBINED products are estimated by error propagation.

In this thesis, the ESA CCI SM ACTIVE version 08.1 [49] and ESA CCI SM PASSIVE version 08.1 [50] are used. For the ESA CCI COMBINED product, the rescaling method against long-term Land Surface Model (LSM) based SM (GLDAS-Noah v2.1 [42]) was changed from CDF-matching, which can partly remove the irrigation signal, to mean-standard deviation rescaling, which better preserves seasonal features, in the latest version 09.1 [43]. Hence, to take advantage of this improvement, we decided to use the

[46]: Wagner et al. (1999), 'A Method for Estimating Soil Moisture from ERS Scatterometer and Soil Data'

[47]: Naeimi et al. (2009), 'An Improved Soil Moisture Retrieval Algorithm for ERS and METOP Scatterometer Observations'

[48]: Owe et al. (2008), 'Multisensor historical climatology of satellite-derived global land surface moisture'

[41]: Dorigo et al. (2023), *ESA Climate Change Initiative Plus - Soil Moisture Algorithm Theoretical Baseline Document (ATBD) Supporting Product Version 08.1*

[42]: Rodell et al. (2004), 'The Global Land Data Assimilation System'

[41]: Dorigo et al. (2023), *ESA Climate Change Initiative Plus - Soil Moisture Algorithm Theoretical Baseline Document (ATBD) Supporting Product Version 08.1*

[49]: Dorigo et al. (2023), 'ESA Soil Moisture Climate Change Initiative (Soil Moisture cci): ACTIVE product, Version 08.1'

[50]: Dorigo et al. (2023), 'ESA Soil Moisture Climate Change Initiative (Soil Moisture cci): PASSIVE product, Version 08.1'

[43]: Dorigo et al. (2024), *ESA Climate Change Initiative Plus - Soil Moisture Algorithm Theoretical Baseline Document (ATBD) Supporting Product Version 09.0*

Die approbierte gedruckte Originalversion dieser Diplomarbeit ist an der TU Wien Bibliothek verfügbar
The approved original version of this thesis is available in print at TU Wien Bibliothek.
TU Bibliothek Your knowledge hub WIEN

ESA CCI COMBINED SM version 09.1 product [51].

[51]: Dorigo et al. (2024), 'ESA Soil Moisture Climate Change Initiative (Soil Moisture cci): COMBINED product'

SMOS

The Soil Moisture and Ocean Salinity (SMOS) [52] mission of ESA's Living Planet Programme, launched in 2009, is the first satellite mission dedicated to SM observation. [53] It provides global observations of variability in SM and sea surface salinity at an average spatial resolution of 42 km and global coverage every 3 days. The instrument installed is a Microwave Imaging Radiometer using Aperture Synthesis (MIRAS). It is a passive microwave 2-D interferometric microwave radiometer that receives radiation from the Earth at a frequency of 1.4 GHz in the L-band. The measured signal is then related to the moisture content in the topsoil layer (0 to 5 cm depth). [52]

[52]: Kerr et al. (2001), 'Soil moisture retrieval from space: The Soil Moisture and Ocean Salinity (SMOS) mission'

[53]: Kerr et al. (2016), 'Overview of SMOS performance in terms of global soil moisture monitoring after six years in operation'

SMAP

NASA's Soil Moisture Active Passive (SMAP) satellite mission was designed to retrieve SM from active and passive L-band microwave sensors [54]. Shortly after its launch in January 2015, however, the active sensor failed and hence SMAP only provides surface SM up to a depth of 5 cm remotely sensed by the passive microwave radiometer [29]. SMAP's radiometric-based instrument detects radio waves emitted by the Earth at a frequency of 1.4 GHz in L-band. The SMAP Level 2 SM data used in this thesis are provided with a spatial resolution of 40 km sampled on a 36-km grid and an average global revisit time of 3 days [54].

[54]: Entekhabi et al. (2010), 'The Soil Moisture Active Passive (SMAP) Mission'

[29]: Brocca et al. (2015), 'Rainfall estimation from in situ soil moisture observations at several sites in Europe: an evaluation of the SM2RAIN algorithm'

[54]: Entekhabi et al. (2010), 'The Soil Moisture Active Passive (SMAP) Mission'

Modeled soil moisture

ERA5-Land

The land component of the fifth generation of the European ReAnalysis (ERA5-Land) is produced by the Copernicus Climate Change Service (C3S) at the European Centre for Medium-Range Weather Forecasts (ECMWF) [55]. The period covered by the data set extends from 1950 to the present. ERA5-Land describes the water and energy cycles over land at a spatial resolution of 9 km and hourly time steps. First, the coarser ERA5 meteorological data, with a resolution of 31 km, are downscaled to a spatial resolution of 9 km. Then, the land surface model uses a daily lapse rate from ERA5 to correct the meteorological forcing data. Finally, a 24-hour integration is performed to provide the evolution of the land surface state and the associated energy and water fluxes [56]. As ERA5-Land is a reanalysis product, driven by meteorological forcing, it does not contain an irrigation signal [34]. To match the sensor depth of the satellite SM data, only the volumetric soil water layer 1 (0-7 cm) is considered [56].

[55]: Muñoz-Sabater (2019), 'ERA5-Land hourly data from 1950 to present'

[34]: Zohaib et al. (2020), 'Satellite-based global-scale irrigation water use and its contemporary trends'

2.2.2 In situ irrigation data

Ebro Basin

Irrigation benchmark data within the Ebro Basin are available for irrigated land organized into five irrigation districts, namely Urgell, Algerri Balaguer, Pinyana, and the Catalan and Aragonese district, which is divided into North and South (Figure 2.3). Daily data are available from

Figure 2.3: Irrigated districts with available in situ data in the Ebro Basin.

Die approbierte gedruckte Originalversion dieser Diplomarbeit ist an der TU Wien Bibliothek verfügbar
The approved original version of this thesis is available in print at TU Wien Bibliothek.
TU Bibliothek Your knowledge hub WIEN

Table 2.2: Overview of the irrigation districts in the Ebro Basin as in Dari et al. [32].

District name	Area km^2	Loss factor	Irrigation technique
Algerri Balaguer	71	10%	sprinkler and drip irrigation
Catalan and Aragonese North	657	15%	sprinkler (54 %), drip (28 %)
Catalan and Aragonese South	504	15%	and flood (18 %) irrigation
Pinyana	150	30%	mixed irrigation
Urgell	812	30%	mostly flood irrigation

[32]: Dari et al. (2020), 'Exploiting High-Resolution Remote Sensing Soil Moisture to Estimate Irrigation Water Amounts over a Mediterranean Region'

[57]: SAIH (), *Sistema automatico de Informacion Hidrologica del Ebro*

2007 to 2023 for Algerri-Balaguer and Catalan and Aragonese North, and from 1997 to 2023 for Catalan and Aragonese South and Urgell. Monthly data for the Pinyana district are available for 2016 and 2017 [32]. The districts vary in size and irrigation system (see Table 2.2), which results in different irrigation efficiencies generating more or less water loss, which was accounted for in the in situ irrigation data provided. Urgell is the largest district covering an area of about 812 km^2. It is mainly irrigated by flood irrigation, which is an old irrigation technique generating more losses by drainage and runoff compared to modern irrigation techniques. Consequently, losses of 30 % are generally considered [32]. The Catalan and Aragonese North and South districts cover similarly large areas of 657 km^2 and 504 km^2, respectively. Irrigation systems are mixed, but sprinkler (54 %), drip (28 %), and flood (18 %) irrigation are the most common [32]. Losses of 15 % are considered for both the northern and southern districts. The smallest district, covering only about 70 km^2, is Algerri-Balaguer. It is the most modern and efficient of the five irrigation districts and is equipped with recently installed sprinkler and drip irrigation systems. Losses are assumed to be only 10 % for Algerri-Balaguer. In the districts described so far, all in situ irrigation data are provided daily by the Automatic Hydrologic Information System of the Ebro River Basin (SAIH Ebro, [57]). For the Pinyana district, with an area of approximately 1150 km^2, data are provided monthly by the canal's technical office.

Irrigation water is distributed to the five irrigation districts through canals. The volume of the water through-flow is measured just upstream of the districts and is converted into water thickness (mm) by dividing by the area of each irrigation district. Figure 2.3 shows the location of the five districts within the Ebro Basin. Given the surface area of the irrigation districts and the coarse resolution (0.25°) of the SM satellite and model pixels, we decided to carry out the validation on this area using the average of the in situ data from four districts, excluding Pinyana due to the limited availability of in situ data over time.

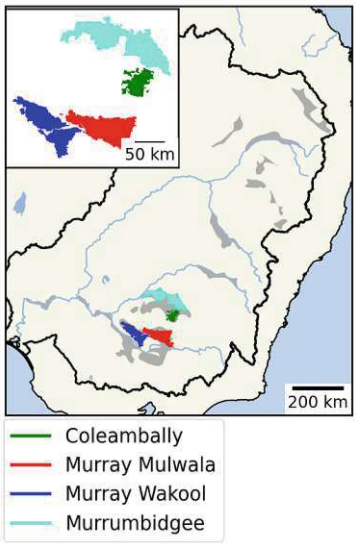

Figure 2.4: Irrigated districts with available in situ data in the Murray-Darling Basin.

Murray-Darling Basin

For the Murray-Darling Basin, monthly irrigation benchmark data, expressed as monthly water thickness (mm/month), is available for five districts (see Table 2.3, with four of them being illustrated in Figure 2.4.

The data set of the Coleambally district with an area of 977 km^2 covers a period from July 2009 to June 2019. Irrigation data in Murray Mulwala and Murray Wakool with areas of 3093 km^2 and 1455 km^2, respectively, are available from July 2010 to June 2019. Benchmark irrigation data in Murrumbidgee is available from July 2013 to June 2019. The Murrumbidgee

Die approbierte gedruckte Originalversion dieser Diplomarbeit ist an der TU Wien Bibliothek verfügbar
The approved original version of this thesis is available in print at TU Wien Bibliothek.
TU Bibliothek Your knowledge hub WIEN

district covers an area of approximately 2790 km^2. The monthly irrigation data are provided by an Irrigation Infrastructure Operator (IIO) in the form of annual reports. The discharge ($m^3/month$) values measured upstream of each district are divided by the irrigated area to obtain water thickness in mm/month. [30]

[30]: Dari et al. (2023), 'Regional data sets of high-resolution (1 and 6 km) irrigation estimates from space'

District name	Area km^2	Time span
Coleambally	977	2009-2009
Murrumbidgee	2789	2013-2019
Murray Mulwala	3093	2010-2019
Murray Wakool	1455	2010-2019

Table 2.3: Overview of the irrigation districts in the Murray-Darling Basin as in Dari et al. (2023) [30].

2.2.3 ESA CCI landcover map

The ESA Climate Change Initiative Land Cover (ESA CCI-LC) product provides global land cover maps with a spatial resolution of 300 meters. These maps follow the typology defined by the Land Cover Classification System (LCCS) [58], developed by FAO. Annual land cover maps are derived from a foundational LC map based on the complete Envisat Medium Resolution Imaging Spectrometer (MERIS) Full Resolution (FR) and Reduced Resolution (RR) archives [59].

In this study, we used mask 20 from the "level 1" or "global" legend, which is globally valid and represents irrigated cropland worldwide [60]. We spatially resampled the land cover data from 300 m to the 0.25° ESA CCI grid, keeping only those pixels with at least 10 % of their area classified as irrigated cropland.

[58]: Jansen et al. (2000), *Land Cover Classification System (LCCS): Classification Concepts and User Manual*

[59]: Bezy et al. (1999), *Medium resolution imaging spectrometer (MERIS)*

[60]: Defourny et al. (2017), *CCI Land Cover Product User Guide v2*

Die approbierte gedruckte Originalversion dieser Diplomarbeit ist an der TU Wien Bibliothek verfügbar
The approved original version of this thesis is available in print at TU Wien Bibliothek.
TU Bibliothek Your knowledge hub WIEN

Die approbierte gedruckte Originalversion dieser Diplomarbeit ist an der TU Wien Bibliothek verfügbar
The approved original version of this thesis is available in print at TU Wien Bibliothek.

Methods 3

3.1 Preprocessing

3.1.1 Spatial resampling

All SM satellite and modeled SM estimates were resampled to the 0.25° ESA CCI SSM v08.1 grid [61], using linear interpolation. Moreover, all data available on a sub-daily basis, particularly ERA5-Land, were temporally resampled to daily time steps.

[61]: Hirschi et al. (2023), 'ESA Climate Change Initiative Plus - Soil Moisture Product Validation and Intercomparison Report (PVIR) Supporting Product version v08.1 (issue 1.0)'

3.1.2 Rescaling

Observation depths and units employed differ between the different products. The ERA5-Land volumetric soil water layer 1, for instance, is modeled for a depth of up to 7 cm [55] and is provided in volumetric units m^3m^{-3}, whereas the SM product provided by ESA CCI ACTIVE represents approximately the 0-5 cm topsoil layer in degrees of saturation % [61].

[55]: Muñoz-Sabater (2019), 'ERA5-Land hourly data from 1950 to present'

Consequently, each satellite time series is rescaled to the modeled SM time series ERA5-Land. The rescaling is a crucial and non-trivial step that can have a significant impact on the simulated irrigation. We employed two distinct rescaling methodologies, the "mean-standard deviation" rescaling and "1%-99%-quantile" rescaling, and investigated which approach is more appropriate. The following section presents an overview of the two rescaling methods.

"Mean-standard deviation" rescaling method

The "mean-standard deviation" rescaling method has been widely used (see for example Zaussinger et al. (2019) [25] and Escorihuela et al. (2016) [62]). It is a linear rescaling technique that aligns the satellite SM time series SM_{sat}, with the same mean μ and standard deviation σ, as the modeled SM time series SM_{mod}. This methodology is expressed in Equation 3.1:

[25]: Zaussinger et al. (2019), 'Estimating irrigation water use over the contiguous United States by combining satellite and reanalysis soil moisture data'

[62]: Escorihuela et al. (2016), 'Comparison of remote sensing and simulated soil moisture datasets in Mediterranean landscapes'

$$SM^{sat}_{rescaled} = \frac{SM^{sat} - \mu(SM^{sat})}{\sigma(SM^{sat})}\sigma(SM^{mod}) + \mu(SM^{mod}). \tag{3.1}$$

Over irrigated areas, $mu(SM^{sat}$ likely increases during irrigation periods, altering scaling parameters. While this should not affect the temporal evolution of SM changes, the impact of irrigation on temporal variability introduces uncertainty, especially in very dry regions where model SM may not reach saturation, but remotely sensed data might due to irrigation.

Die approbierte gedruckte Originalversion dieser Diplomarbeit ist an der TU Wien Bibliothek verfügbar
The approved original version of this thesis is available in print at TU Wien Bibliothek.
TU Bibliothek Your knowledge hub WIEN

"1%-99%-quantile" rescaling method

The objective of the quantile rescaling method is to align the 1 % and 99 % quantiles of the satellite SM time series with the 1 % and 99 % quantiles of the modeled SM time series [63]. The concept is illustrated in Equation 3.2. Escorihuela et Quintana (2016) [62] highlight that the limitation of this normalization method is the need for a long time series to ensure that the satellite and modeled SM reach their maximum and minimum values during the period considered and that the method is susceptible to extreme values. However, compared to mean-standard rescaling, this method has the advantage of being less sensitive to seasonal variability caused by irrigation.

[63]: Brocca et al. (2011), 'Soil moisture estimation through ASCAT and AMSR-E sensors: An intercomparison and validation study across Europe'

[62]: Escorihuela et al. (2016), 'Comparison of remote sensing and simulated soil moisture datasets in Mediterranean landscapes'

$$SM^{sat}_{rescaled} = \frac{SM^{sat} - SM^{sat}_{Q0.01}}{SM^{sat}_{Q0.99} - SM^{sat}_{Q0.01}}(SM^{mod}_{Q0.99} - SM^{mod}_{Q0.01}) + SM^{mod}_{Q0.01}. \quad (3.2)$$

where the index $Q0.01$ indicates the value of the 1 % quantile and the index $Q0.99$ indicates the value of the 99 % quantile.

3.1.3 Masking

Pixels with at least 10 % of their area classified as irrigated cropland by the ESA CCI land cover map are retained to ensure the presence of an irrigation signal.

3.2 Statistical analysis of soil moisture data

3.2.1 Kolmogorov-Smirnov test

Prior to computing IWU, we validated our assumption that satellite-derived SM data capture an irrigation signal, while modeled SM data remain unaffected by irrigation. To assess this, we performed a Kolmogorov-Smirnov (KS) test. The KS-test is a statistical tool that assesses the empirical distribution functions of two or more time series data sets. It has been employed in numerous studies, including Kumar et al. (2015) [20], Zohaib et Choi (2020) [34] and Nair et al. (2019) [64]. The null hypothesis (H_0) states that the two SM datasets have similar distributions, while the alternative hypothesis (H_a) postulates that the two distributions are different. The two empirical distribution functions, designated as $F_1(x)$ and $F_2(x)$ are calculated, and the absolute difference between them is determined as follows:

[20]: Kumar et al. (2015), 'Evaluating the utility of satellite soil moisture retrievals over irrigated areas and the ability of land data assimilation methods to correct for unmodeled processes'

[34]: Zohaib et al. (2020), 'Satellite-based global-scale irrigation water use and its contemporary trends'

[64]: Nair et al. (2019), 'Improvement of land surface model simulations over India via data assimilation of satellite-based soil moisture products'

$$D_{m,n} = max_x|F_1(x) - F_2(x)| \quad (3.3)$$

where m and n represent the sample sizes of F_1 and F_2, respectively. A similar distribution of the two SM datasets is indicated by KS statistic values (D) close to zero. Conversely, significant differences in the distributions are represented by higher values of D. Higher D values during the irrigated period suggest differences in the distributions, indicating

Die approbierte gedruckte Originalversion dieser Diplomarbeit ist an der TU Wien Bibliothek verfügbar
The approved original version of this thesis is available in print at TU Wien Bibliothek.
TU Bibliothek Your knowledge hub WIEN

the presence of an irrigation signal in the satellite SM data. Thus, this metric serves as an indicator for assessing the suitability of a satellite SM product for irrigation retrieval.

3.2.2 Statistical metrics

In addition to the Kolmogorov-Smirnov test the statistical metrics bias, Root-Mean-Squared-Deviation (RMSD), and Pearson correlation coefficient (R) are computed between ERA5-Land SM and the various satellite SM data sets to further assess the potential of SM satellite products to detect irrigation. The statistical metrics are defined as follows [34]:

[34]: Zohaib et al. (2020), 'Satellite-based global-scale irrigation water use and its contemporary trends'

$$bias = \frac{1}{n}\sum_{i=1}^{n}(SM_i^{sat} - SM_i^{mod}) \tag{3.4}$$

$$RMSD = \sqrt{\frac{1}{n}\sum_{i=1}^{n}(SM_i^{mod} - SM_i^{sat})^2} \tag{3.5}$$

$$R = \frac{\sum_{i=1}^{n}(SM_i^{sat} - \overline{SM_i^{sat}})(SM_i^{mod} - \overline{SM_i^{mod}})}{\sqrt{\sum_{i=1}^{n}(SM_i^{sat} - \overline{SM_i^{sat}})^2}\sqrt{\sum_{i=1}^{n}(SM_i^{mod} - \overline{SM_i^{mod}})^2}} \tag{3.6}$$

The bias is calculated as the average difference between satellite and modeled SM values, where positive values suggest that the satellite SM estimates are generally higher than those from the model, while negative values indicate that the model provides higher SM values on average. The bias serves to highlight systematic deviations between the datasets and provides insight into persistent under- or overestimation trends.

The RMSD quantifies the typical magnitude of differences between satellite and modeled SM values, where smaller RMSD values suggest a closer agreement between the two datasets. Larger RMSD values, by contrast, indicate a broader spread and reduced alignment in SM estimates, reflecting less consistency between the satellite and model data.

The Pearson correlation coefficient, ranging from -1 to 1, measures the strength and direction of the linear relationship between the satellite and modeled SM dynamics. A coefficient close to 1 implies a strong positive correlation, where satellite and model SM values increase or decrease together, while values near -1 suggest a strong inverse relationship. Correlation values close to 0 indicate weak or no linear relationship, meaning the datasets vary independently.

All three statistical metrics help determine the presence of an irrigation signal, providing valuable insights into which of the five satellite SM products are strong candidates for irrigation retrieval.

3.3 Observation frequency

Zappa et al. (2022) [27] showed that the performance of the SM Delta algorithm decreases significantly when the SM frequency is greater than 3 days. Furthermore, they point out that the performance of the algorithm

[27]: Zappa et al. (2022), 'How accurately can we retrieve irrigation timing and water amounts from (satellite) soil moisture?'

Die approbierte gedruckte Originalversion dieser Diplomarbeit ist an der TU Wien Bibliothek verfügbar
The approved original version of this thesis is available in print at TU Wien Bibliothek.
TU Bibliothek Your knowledge hub WIEN

is best with daily observations and drops off sharply when observations are available less than every third day. Given the sensitivity of the SM Delta algorithm to the number of observations available, an analysis has been conducted on the measurement frequency of the various satellites. Hence, spatial maps of the observation frequency estimations have been computed for the various sites, representing the number of observations per year. This analysis helps identify the satellite-based products most suitable for accurately retrieving irrigation data.

3.4 The SM Delta approach

The SM Delta approach, which was developed by Zaussinger et al. (2019) [25] over the CONUS, then globally expanded by Zohaib et Choi (2020) [34] and further investigated by Zappa et al. (2021, 2022, 2024) [26–28], aims to retrieve irrigation based on the difference in satellite and modeled SM variations. It takes advantage of the fact that modeled SM, if irrigation is not modeled, theoretically only contains precipitation signals [34] (see Equation 3.8), whereas satellite SM additionally contains an irrigation signal [65], [34] (see Equation 3.7).

Zaussinger et al. (2019) [25] proposed defining an irrigation event as occurring when there is a simultaneous increase in satellite-derived SM ($\frac{dSM_{sat}}{dt} > 0$) and either a decrease or no change in model-based SM ($\frac{dSM_{mod}}{dt} \leq 0$). Hereby, it can be assured that the increase in satellite SM is very likely a result of an irrigation event and not caused by precipitation. The SM Delta method is based on the soil water balance equations, which describe the respective change in SM for each time step t (day).

The equations are expressed as

$$Z^* \frac{dSM_{sat}}{dt} = P(t) + I(t) - ET(t) - R(t) - \Delta S_{rest} \tag{3.7}$$

for the satellite observation and as

$$Z^* \frac{dSM_{mod}}{dt} = P(t) - ET(t) - R(t) - \Delta S_{rest} \tag{3.8}$$

for the model simulation.

Where Z^* is the soil depth considered in mm, SM_{sat} represents the satellite SM in volumetric units m^3m^{-3}, SM_{mod} is the modeled SM in volumetric units m^3m^{-3}, P represents precipitation in mm, I is irrigation in mm, ET is evapotranspiration, which is the evaporation of soil and transpiration of vegetation, in mm, R is the runoff in mm and ΔS_{rest} is the change in water storage m^3m^{-3} beneath the topsoil layer [25, 34].

The amount of irrigation water per event is calculated as the difference between the change in satellite and model SM within a certain time step. The fundamental assumption of the SM Delta approach, as proposed by Zaussinger et al. (2019) [25], is that the discrepancies between the model and satellite observations in terms of ET, P, R, and ΔS can be considered negligible and therefore be disregarded. This results in the following equation calculating the IWU by subtracting Equation 3.8 from Equation 3.7.

[25]: Zaussinger et al. (2019), 'Estimating irrigation water use over the contiguous United States by combining satellite and reanalysis soil moisture data'

[34]: Zohaib et al. (2020), 'Satellite-based global-scale irrigation water use and its contemporary trends'

[26]: Zappa et al. (2021), 'Detection and Quantification of Irrigation Water Amounts at 500 m Using Sentinel-1 Surface Soil Moisture'

[27]: Zappa et al. (2022), 'How accurately can we retrieve irrigation timing and water amounts from (satellite) soil moisture?'

[28]: Zappa et al. (2024), 'Benefits and pitfalls of irrigation timing and water amounts derived from satellite soil moisture'

[65]: Lawston et al. (2017), 'Irrigation Signals Detected From SMAP Soil Moisture Retrievals'

[25]: Zaussinger et al. (2019), 'Estimating irrigation water use over the contiguous United States by combining satellite and reanalysis soil moisture data'

Die approbierte gedruckte Originalversion dieser Diplomarbeit ist an der TU Wien Bibliothek verfügbar
The approved original version of this thesis is available in print at TU Wien Bibliothek.
TU Bibliothek Your knowledge hub WIEN

$$I(t) = Z^* \frac{dSM_{sat}}{dt} - Z * \frac{dSM_{mod}}{dt} \tag{3.9}$$

In addition, a threshold parameter is introduced, as proposed by Zaussinger et al. (2019) [25], which allows to ensure that the change in satellite SM is significant to be considered as irrigation. Indeed, there is noise present in the SM signals [66], and distinguishing between the irrigation signal and the high-frequency noise is essential to the algorithm. Accordingly, the relative change in satellite SM between two time steps is calculated, and the retrieved irrigation is only considered if the relative change exceeds a certain threshold, as illustrated in Equation 3.10. Zaussinger et al. (2019) [25] performed an extensive sensitivity analysis and concluded that a threshold of 0.12 yields the optimal results. Thus, this study uses 0.12 as the threshold value, following the finding of Zaussinger et al. (2019).

[25]: Zaussinger et al. (2019), 'Estimating irrigation water use over the contiguous United States by combining satellite and reanalysis soil moisture data'

[66]: Dorigo et al. (2010), 'Error characterisation of global active and passive microwave soil moisture datasets'

$$\frac{SM_t^{sat} - SM_{t-n}^{sat}}{SM_{t-n}^{sat}} \geq 0.12 \equiv thresh. \tag{3.10}$$

The seasonal IWU is subsequently calculated as the aggregated difference of the change in satellite and model SM for irrigation events exceeding the determined threshold within the growing season period.

$$IWU_{seas} = \int_{i_{SOS}}^{i_{EOS}} (dSM_i^{sat} - dSM_i^{mod})dt \approx \sum_{i=SOS}^{EOS} \Delta SM_i^{sat-mod} \tag{3.11}$$

where

$$\Delta SM_i^{sat-mod} = \begin{cases} \Delta SM_i^{sat} - \Delta SM_i^{mod}, & if\ \Delta SM_i^{sat} \geq thresh \\ 0, & otherwise \end{cases}$$

$$\Delta SM_i^{sat} = SM_i^{sat} - SM_{i-n}^{sat}$$
$$\Delta SM_i^{mod} = SM_i^{mod} - SM_{i-n}^{mod}$$

with i_{SOS} and i_{EOS} representing the start and end of irrigation season respectively. SM_i and SM_{i-n} represent the SM observation on day i and the last available SM observation n days before. Note that if the satellite data frequency is larger than 4 days, it is not possible to say with certainty whether the increase in satellite SM is due to irrigation or precipitation. Therefore, when the gaps between two observations exceed 4 days, this period is conservatively disregarded.

3.5 Area factor for validation

Validation data are available for irrigation districts covered by multiple 0.25° pixels. While some pixels are fully contained within the district boundaries, others only partially overlap, resulting in a theoretically weaker irrigation signal in those pixels. To address this variation in pixel coverage and the resulting underestimation of irrigation values, the average IWU of all the pixels including a portion of an irrigation district is calculated, and a spatial adjustment factor is applied to this average.

Die approbierte gedruckte Originalversion dieser Diplomarbeit ist an der TU Wien Bibliothek verfügbar
The approved original version of this thesis is available in print at TU Wien Bibliothek.
TU Bibliothek Your knowledge hub WIEN

To do so, the intersection area between the pixel and the irrigated area is computed for each pixel. Then, the conversion factor is calculated as the division of the area of the pixel and the intersection area as shown in Equation 3.12.

$$f_{i,\,area} = \frac{A_{pixel}}{A_{i,\,intersect}} \tag{3.12}$$

where $A_{pixel}\ in\ m^2$ is the area of a 0.25° pixel, and $A_{i,\,intersect}\ in\ m^2$ is the intersecting area between the pixel i and the irrigation district.

The conversion factor $f_{i,\,area}$ is then applied to the IWU of the pixel i by multiplying the original time series by the computed conversion factor (compare Equation 3.13).

$$IWU_{i,\,factor} = IWU_{i,\,original} * f_{i,\,area} \tag{3.13}$$

Furthermore, the weight of the pixel i is calculated by dividing the intersection area of the pixel with the irrigated area $A_{i,\,intersect}$ by the whole irrigated area $A_{irrigated}$:

$$weight_i = \frac{A_{intersect,i}}{A_{irrigated}} \tag{3.14}$$

The total IWU is then calculated as the sum of the weighted IWU values for each district, where each IWU value is multiplied by its corresponding weight:

$$IWU = \sum_{i=1}^{n} IWU_{i,\,factor} * weight_i \tag{3.15}$$

In the Murray-Darling Basin, the extension of the irrigated area underwent changes over the years analyzed. To account for the alterations in the irrigated area, the conversion factor, designated as f_{area}, was calculated for three distinct time periods and applied individually. The first period includes the years before 2013, the second period ranges from 2013 to 2016 and the third period includes the years 2017 to 2019. Additionally, the weights were calculated and applied separately.

Die approbierte gedruckte Originalversion dieser Diplomarbeit ist an der TU Wien Bibliothek verfügbar
The approved original version of this thesis is available in print at TU Wien Bibliothek.
TU Bibliothek Your knowledge hub WIEN

Results 4

4.1 Rescaling

To select the most appropriate rescaling method, we performed a visual assessment of the rescaled time series obtained with both rescaling methodologies over about 60 pixels spread over the two study areas. To illustrate the effect of scaling on SM time series, Figures 4.1a to 4.1e show the original (gray lines), rescaled (dotted orange for the "mean-standard deviation" and dotted green for the "1%-99%-quantile" rescaling method) and modeled (ERA5-Land, blue line) SM time series. Figures 4.1a, 4.1b and 4.1c show these SM time series for an irrigated pixel in the Ebro Basin for ESA CCI COMBINED, SMOS, and ESA CCI ACTIVE, respectively. Figures 4.1d and 4.1e show the effect of rescaling for an irrigated pixel in the Murray-Darling Basin for ESA CCI PASSIVE and ESA CCI COMBINED, respectively. We see that both methods have a clear impact on the SM time series, particularly visible in Figures 4.1b, 4.1d and 4.1e, showing that without rescaling, the satellite SM is systematically lower than the model SM. Furthermore, we can see that both rescaling methods ("mean-standard deviation" and "1%-99%-quantile") modify the SM time series in a fairly similar way in the Figures 4.1a to 4.1e. In addition, literature suggests that the mean-standard rescaling method is less prone to extreme values [62, 67]. Consequently, we decided to use the mean-standard rescaling method for this study.

[62]: Escorihuela et al. (2016), 'Comparison of remote sensing and simulated soil moisture datasets in Mediterranean landscapes'
[67]: Brocca et al. (2013), 'Scaling and Filtering Approaches for the Use of Satellite Soil Moisture Observations'

Die approbierte gedruckte Originalversion dieser Diplomarbeit ist an der TU Wien Bibliothek verfügbar
The approved original version of this thesis is available in print at TU Wien Bibliothek.

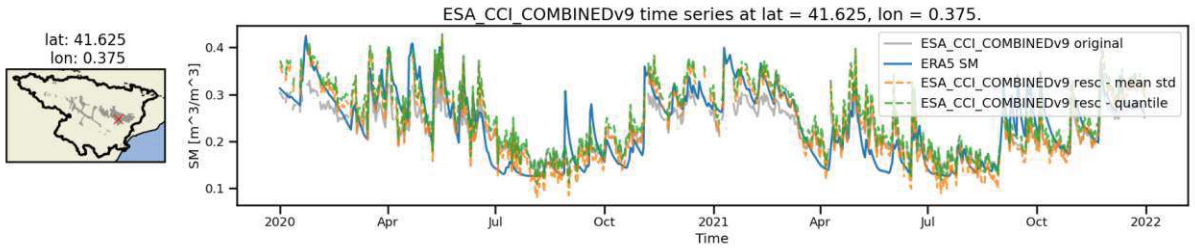

(a) Rescaling ESA CCI COMBINED time series to ERA5-Land SM using mean-std-rescaling and quantile rescaling.

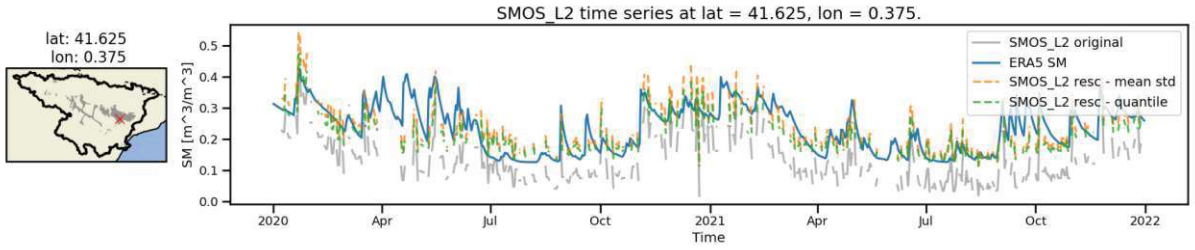

(b) Rescaling SMOS time series to ERA5-Land SM using mean-std-rescaling and quantile-rescaling.

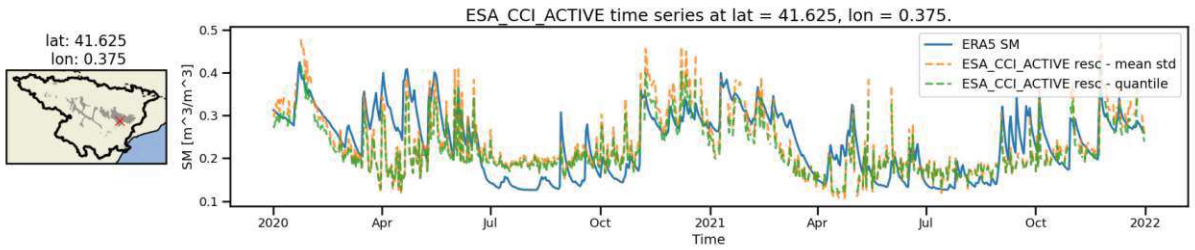

(c) Rescaling ESA CCI ACTIVE time series to ERA5-Land SM using mean-std-rescaling and quantile-rescaling. The original ESA CCI ACTIVE SM time series is not shown, as it is provided in % and the values are in a range not comparable to the rescaled SM time series.

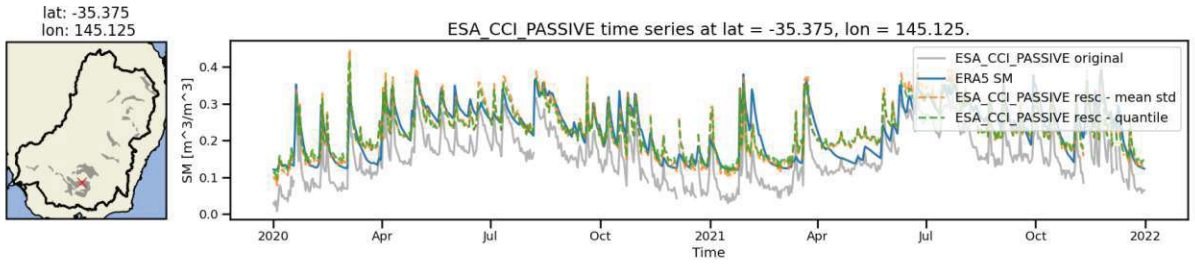

(d) Rescaling ESA CCI PASSIVE time series to ERA5-Land SM using mean-std-rescaling and quantile-rescaling.

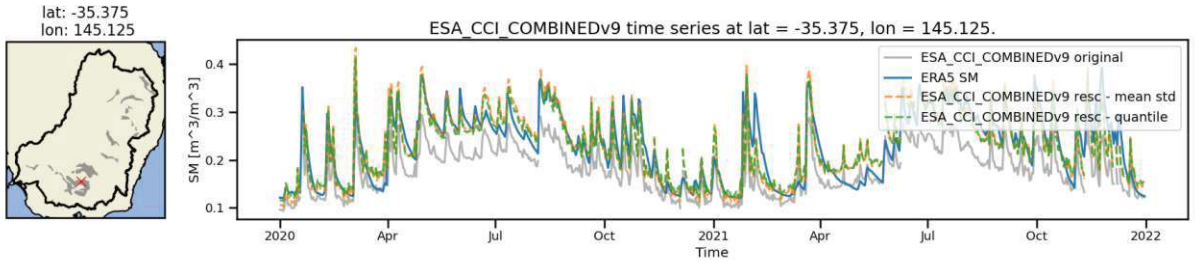

(e) Rescaling ESA CCI COMBINED time series to ERA5-Land SM using mean-std-rescaling and quantile-rescaling.

Figure 4.1: Rescaling satellite SM time series to ERA5-Land SM using mean-std-rescaling and quantile-rescaling in the Ebro Basin and the Murray-Darling Basin.

Die approbierte gedruckte Originalversion dieser Diplomarbeit ist an der TU Wien Bibliothek verfügbar
The approved original version of this thesis is available in print at TU Wien Bibliothek.
TU Bibliothek Your knowledge hub WIEN

4.2 Spatial analysis of the soil moisture products

In order to assess the difference between satellite SM and model SM and to evaluate the potential of different satellite-model pairs to retrieve irrigation, a spatial analysis was carried out. It consisted of computing four different metrics (KS test, RMSD, Pearson correlation, and bias) on agricultural pixels and only on non-rainy days during the irrigation season, i.e. the periods when the difference in SM between satellite and model due to irrigation is expected to be most significant. The non-irrigation season has also been analyzed for comparison. Figures 4.2a to 4.5b show the KS-test, RMSD, bias, and Pearson correlation on non-rainy days during the irrigation season in the Ebro and Murray-Darling basins using the ESA CCI COMBINED and ACTIVE products and ERA5-Land SM. Furthermore, all the computed metrics are summarized in Tables 4.1 and 4.2 for non-rainy days during the irrigation and non-irrigation seasons, respectively.

It is anticipated that the KS test will yield higher values (closer to 1) on dry days during the irrigation season, when distributions are distinct due to the irrigation signal being only present in the satellite time series, than on dry days during the non-irrigated season, when values closer to 0 are expected. This expectation is met partially in the Ebro Basin, where ESA CCI COMBINED, ESA CCI ACTIVE, and SMAP exhibit higher KS values during the irrigated season ($KS_{COMBINED} = 0.19$, $KS_{ACTIVE} = 0.32$, $KS_{SMAP} = 0.22$) in comparison to the non-irrigated season ($KS_{COMBINED} = 0.15$, $KS_{ACTIVE} = 0.21$, $KS_{SMAP} = 0.17$) (see Figure 4.2a and Table 4.1). A clearer picture is drawn in the Murray-Darling Basin, where higher KS values are obtained for the irrigated season in comparison to the non-irrigated season for all five satellite products. The ESA CCI ACTIVE product (Figures 4.2b and 4.2c and Table 4.2), exhibits the highest KS value ($KS_{ACTIVE} = 0.32$ in the Ebro Basin and $KS_{ACTIVE} = 0.28$ in the Murray-Darling Basin), indicating the most distinct distribution between the satellite and modeled SM in both basins.

The second metric computed is the RMSD. As a reminder, we expect to see higher values during the irrigation period in comparison to the non-irrigated season. A comparison of the RMSD values computed for the two seasons and presented in Figure 4.3, showing the metric between ESA CCI COMBINED and ERA5-Land SM in the Ebro Basin, did not yield any evidence of an irrigation signal, as the RMSD values were found to be approximately equal. In the Ebro Basin the ESA CCI products have RMSD values of $RMSD_{COMBINED} = 0.054\,m^3/m^3$, $RMSD_{PASSIVE} = 0.060\,m^3/m^3$ and $RMSD_{ACTIVE} = 0.068\,m^3/m^3$ for the irrigated season and RMSD values of $RMSD_{COMBINED} = 0.047\,m^3/m^3$, $RMSD_{PASSIVE} = 0.063\,m^3/m^3$ and $RMSD_{ACTIVE} = 0.052\,m^3/m^3$ for the non-irrigated season. SMOS yields an RMSD value of $RMSD_{SMOS} = 0.051\ m^3/m^3$ for both, the irrigated and the non-irrigated season. The small differences in the RMSD values across both seasons suggest that the model and satellite-derived SM datasets exhibit similar patterns throughout the year, with no identifiable irrigation signal evident from RMSD alone.

Figure 4.4a illustrates the bias between ESA CCI COMBINED and ERA5-Land SM in the Ebro Basin and Figure 4.4b shows the bias between ESA CCI ACTIVE and ERA5-Land SM in the Murray-Darling Basin.

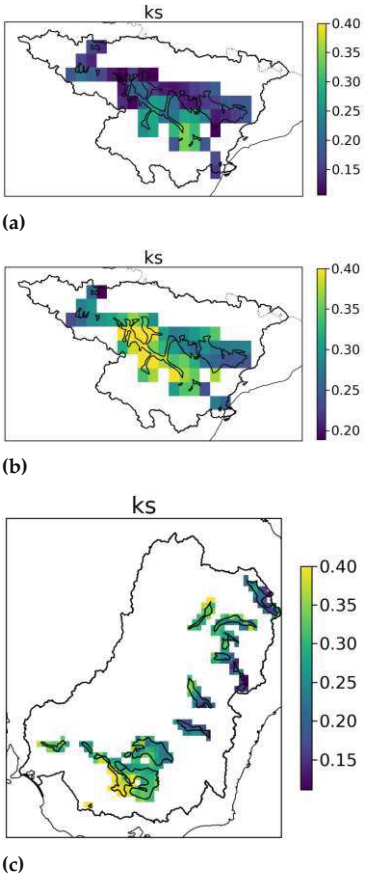

Figure 4.2: KS test [-] (a) between ESA CCI COMBINED SM and ERA5-Land SM in the Ebro Basin, (b) between ESA CCI ACTIVE SM and ERA5-Land SM in the Ebro Basin and (c) between ESA CCI ACTIVE SM and ERA5-Land SM in the Murray-Darling Basin.

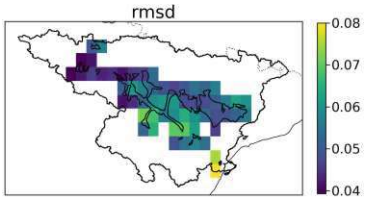

Figure 4.3: RMSD [$m^3 m^{-3}$] between ESA CCI COMBINED SM and ERA5-Land SM in the Ebro Basin.

Die approbierte gedruckte Originalversion dieser Diplomarbeit ist an der TU Wien Bibliothek verfügbar
The approved original version of this thesis is available in print at TU Wien Bibliothek.
TU Bibliothek Your knowledge hub WIEN

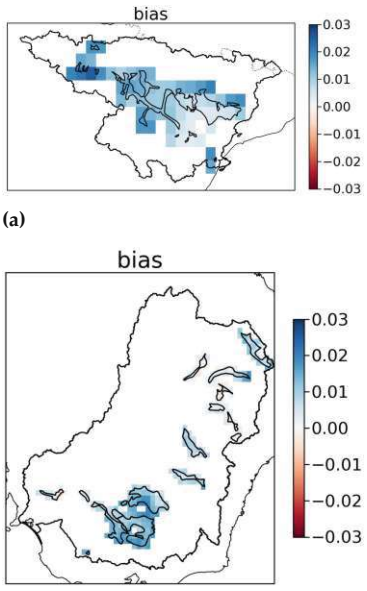

Figure 4.4: Bias [m^3m^{-3}] between (a) ESA CCI COMBINED SM and ERA5-Land SM in the Ebro Basin and (b) ESA CCI ACTIVE SM and ERA5-Land SM in the Murray-Darling Basin.

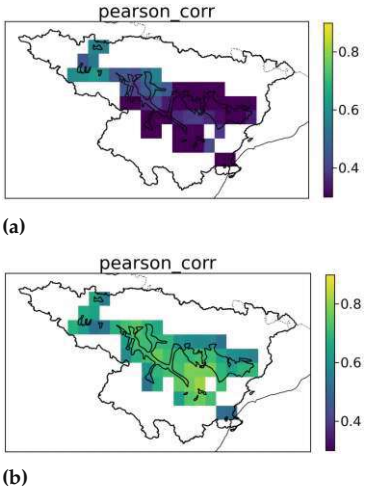

Figure 4.5: Pearson correlation [-] between ESA CCI ACTIVE SM and ERA5-Land SM in the Ebro Basin during (a) the irrigated period and (b) non-irrigated period.

The two plots demonstrate that the satellite SM is wetter than the modeled SM on dry days during the irrigated season in both basins for the respective satellite product. This corresponds to what was expected based on the theoretical assessment. In addition, this is confirmed by the positive averages obtained for the three CCI SM products for the irrigation season ($bias_{COMBINED} = 0.012\ m^3/m^3$, $bias_{PASSIVE} = 0.011\ m^3/m^3$ and $bias_{ACTIVE} = 0.011\ m^3/m^3$). Conversely, during the non-irrigated season, while the ESA CCI COMBINED product yields a similar result of $bias_{COMBINED} = 0.011\ m^3/m^3$, the ESA CCI PASSIVE and ESA CCI ACTIVE products yield negative bias averages of $bias_{PASSIVE} = -0.015\ m^3/m^3$ and $bias_{ACTIVE} = -0.003\ m^3/m^3$, respectively.

It is noteworthy that the ESA CCI products exhibit positive bias values, whereas SMOS and SMAP display negative bias values during the irrigated season for both sites, indicating a lack of irrigation signal (compare Tables 4.1, 4.2 and 4.3). In contrast, the ESA CCI PASSIVE and ESA CCI ACTIVE, as well as the SMOS satellite product, exhibit negative bias values during the non-irrigated season, indicating a higher modeled SM compared to the SM moisture.

The fourth statistical metric analyzed is the Pearson correlation, which is anticipated to be high in the absence of irrigation and lower in case of irrigation events. These expectations are corroborated by all five satellite products within the Murray-Darling Basin, as evidenced by the lower Pearson correlation values observed on dry days during the irrigation season relative to those on dry days during the non-irrigation season (see Table 4.2). In the Ebro Basin, the ESA CCI ACTIVE (Figures 4.5a and 4.5b, $R_{irr} = 0.33$, $R_{non-irr} = 0.67$), SMOS ($R_{irr} = 0.64$, $R_{non-irr} = 0.68$), and SMAP ($R_{irr} = 0.81$, $R_{non-irr} = 0.84$) also exhibit a similar pattern.

Table 4.3 summarizes the differences of the metrics between the irrigated and non-irrigated seasons in both basins. The positive Δ KS values indicate that the distribution of SM during the irrigated season is more different to the modeled SM than the distribution of SM during the non-irrigated season. The ESA CCI ACTIVE product indicates the greatest distinction for this metric. Positive $\Delta RMSD$, as well as positive $\Delta bias$ values indicate that the satellite-derived SM differs greater from the modeled SM during the irrigated season compared to the non-irrigated season. The $\Delta RMSD$ computed from the ESA CCI ACTIVE and ERA5-Land SM products shows the highest difference. However, differences in RMSD are overall small for all five products in both basins. In the Ebro Basin, the $\Delta bias$ computed from ESA CCI PASSIVE and ERA5-Land SM is the largest, indicating that the ESA CCI PASSIVE SM product is a good candidate for retrieving irrigation. In the Murray-Darling Basin, SMOS

Table 4.1: Metrics for the Ebro Basin. KS-test [-]. RMSD in m^3/m^3 , bias in m^3/m^3 and Pearson's correlation [-]

	dry irrigated season				dry non-irrigated season			
satellite	KS	RMSD	bias	Pearson's R	KS	RMSD	bias	Pearson's R
ESA CCI COMBINED	0.19	0.054	0.012	0.70	0.15	0.047	0.011	0.61
ESA CCI PASSIVE	0.20	0.060	0.011	0.64	0.22	0.063	-0.015	0.54
ESA CCI ACTIVE	0.32	0.068	0.011	0.33	0.21	0.052	-0.003	0.67
SMOS	0.19	0.051	-0.005	0.64	0.21	0.051	-0.018	0.68
SMAP	0.22	0.040	-0.004	0.81	0.17	0.037	0.005	0.84

Die approbierte gedruckte Originalversion dieser Diplomarbeit ist an der TU Wien Bibliothek verfügbar
The approved original version of this thesis is available in print at TU Wien Bibliothek.
TU Bibliothek Your knowledge hub WIEN

Table 4.2: Metrics in the Murray-Darling Basin. KS-test [-]. RMSD in m^3/m^3 , bias in m^3/m^3 and Pearson's correlation [-]

	dry irrigated season				dry non-irrigated season			
satellite	KS	RMSD	bias	Pearson's R	KS	RMSD	bias	Pearson's R
ESA CCI COMBINED	0.22	0.036	0.0007	0.80	0.13	0.033	0.005	0.85
ESA CCI PASSIVE	0.21	0.037	0.0009	0.77	0.13	0.034	0.003	0.84
ESA CCI ACTIVE	0.28	0.045	0.0080	0.59	0.17	0.043	0.007	0.75
SMOS	0.22	0.035	-0.0014	0.74	0.15	0.033	-0.005	0.84
SMAP	0.21	0.033	-0.0006	0.77	0.16	0.03	0.006	0.88

Table 4.3: Differences in metrics for the Ebro and Murray-Darling Basins. KS-test [-], RMSD in m^3/m^3, bias in m^3/m^3 and Pearson's correlation [-]. Calculated as irrigated season minus non-irrigated season.

	Ebro Basin				Murray-Darling Basin			
satellite	ΔKS	ΔRMSD	ΔBias	ΔPearson's R	ΔKS	ΔRMSD	ΔBias	ΔPearson's R
ESA CCI COMBINED	0.04	0.007	0.001	0.09	0.09	0.003	-0.0043	-0.05
ESA CCI PASSIVE	-0.02	-0.003	0.026	0.10	0.08	0.003	-0.0021	-0.07
ESA CCI ACTIVE	0.11	0.016	0.014	-0.34	0.11	0.002	0.001	-0.16
SMOS	-0.02	0.000	0.013	-0.04	0.07	0.002	0.0036	-0.10
SMAP	0.05	0.003	-0.009	-0.03	0.05	0.003	-0.0066	-0.11

shows the best potential, when only considering the bias. For the ΔR, the combination of ESA CCI ACTIVE with ERA5-Land SM shows by far the best distinction between irrigated and non-irrigated seasons, indicated by large negative values in Table 4.3.

4.3 Observation frequency

The quantity of available data varies considerably between the satellites and sites. Figure 4.6 shows the observation frequency in the Ebro Basin and Table 4.4 specifies the average number of observations per year for the five analyzed satellites. The ESA CCI COMBINED and ESA CCI PASSIVE satellite products have numerous observations (268 observations/year and 283 observations/year, respectively). Similarly, the ESA CCI ACTIVE product has only slightly fewer observations per year compared to the other two ESA CCI products (245 observations/year). Moreover, the number of measurements made per pixel per year for SMOS and SMAP is on average 202 observations/year and 212 observations/year. The lower number of observations for SMOS and SMAP can be attributed to the longer revisit intervals of these satellites. The ESA CCI COMBINED and the ESA CCI PASSIVE products have the highest observation frequency due to the important number of satellite products they include. Consequently, this analysis shows the considerable potential of ESA CCI COMBINED and ESA CCI PASSIVE in the Ebro Basin compared with the other satellite products.

satellite	counts
ESA CCI ACTIVE	245
ESA CCI PASSIVE	283
ESA CCI COMBINED	268
SMOS	202
SMAP	212

Table 4.4: Yearly number of observations on average in the Ebro Basin.

satellite	counts
ESA CCI ACTIVE	293
ESA CCI PASSIVE	342
ESA CCI COMBINED	336
SMOS	85
SMAP	135

Table 4.5: Yearly number of observations on average in the Murray-Darling Basin.

The context of the Murray-Darling Basin is very different, as depicted in Figure 4.7 and specified in Table 4.5. Compared to the Ebro Basin, the ESA CCI COMBINED and PASSIVE products show significantly higher observation frequencies, with nearly daily observations (335.8 observations/year, and 342 observations/year, respectively). ESA CCI ACTIVE product provides 293 observations per year on average. The

Die approbierte gedruckte Originalversion dieser Diplomarbeit ist an der TU Wien Bibliothek verfügbar
The approved original version of this thesis is available in print at TU Wien Bibliothek.
TU Bibliothek Your knowledge hub WIEN

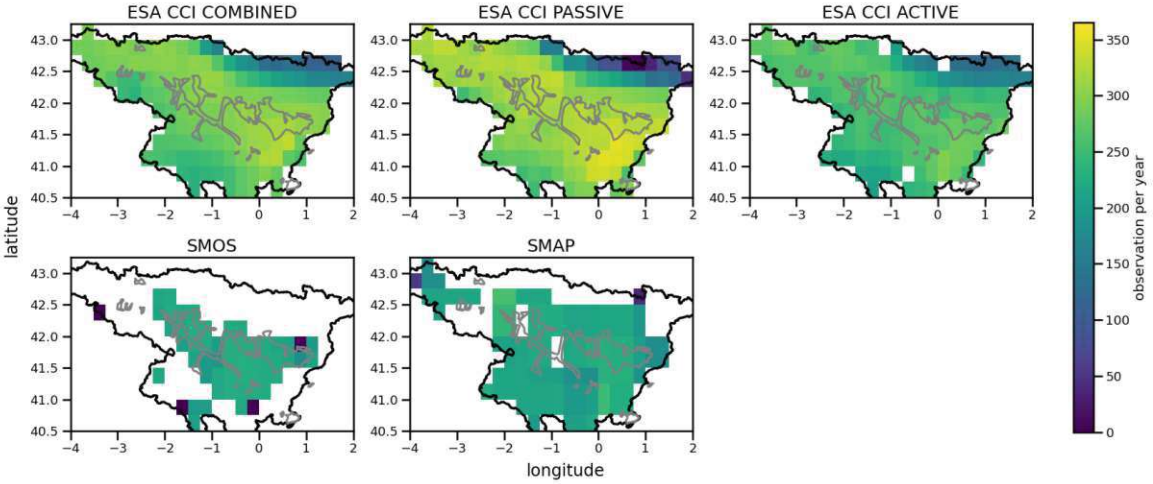

Figure 4.6: Yearly number of observations between 2008 and 2022 for the ESA CCI products, 2010 to 2022 for SMOS and 2015 to 2022 for SMAP over the Ebro Basin.

SMAP and SMOS products show a very different picture. SMAP provides 135 observations/year on average, whereas SMOS exhibits even fewer observations (85 observations/year). The low observation frequency values of SMOS and SMAP are related to the satellites' three-day revisit time and the masking of spurious data. In addition, the data are masked in some irrigated regions. In conclusion, as for the Ebro Basin, the ESA CCI COMBINED and ESA CCI PASSIVE products show the greatest potential compared to the other SM products in the Murray-Darling Basin.

Die approbierte gedruckte Originalversion dieser Diplomarbeit ist an der TU Wien Bibliothek verfügbar
The approved original version of this thesis is available in print at TU Wien Bibliothek.

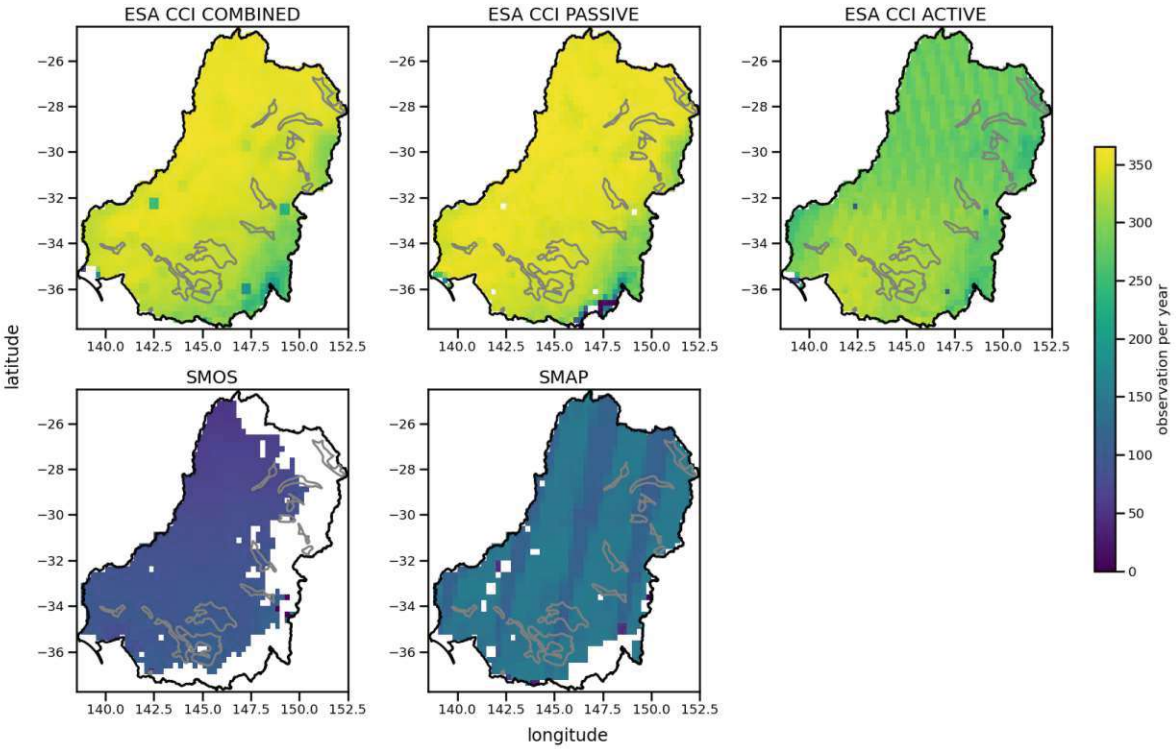

Figure 4.7: Yearly number of observations between 2008 and 2022 for the ESA CCI products, 2010 to 2022 for SMOS and 2015 to 2022 for SMAP over the Murray-Darling Basin.

4.4 Irrigation water use maps

4.4.1 Ebro Basin

Figure 4.8 shows maps of IWU retrieved with the five satellite products, each for the irrigated (left column, March to October) and non-irrigated seasons (right column, November to February) over the Ebro Basin. The three ESA CCI products effectively differentiate between the seasons, with an average IWU of 24.7 mm/month, 24.0 mm/month, and 19.8 mm/month for the ESA CCI PASSIVE, ESA CCI COMBINED, and ESA CCI ACTIVE products, respectively, on average during the irrigated season (Figure 4.8 (a),(c) and (e) and Table 4.6). During the non-irrigated season (Figures 4.8 (b), (d) and (f)) retrieved IWU for the ESA CCI products is lower compared to the irrigated season. The little simulated irrigation during the non-irrigated period might be due to noise in the SM data. However, this thesis focuses on the irrigation period. In contrast, SMOS and SMAP estimate comparable IWU amounts for both irrigated and non-irrigated seasons, albeit slightly higher for the irrigated season. SMAP (Figure 4.8 (g), (h)), generates low values of IWU, amounting to only 7.1 mm/month during the irrigated season and simulates very little irrigation during the non-irrigated season. In comparison, SMOS (Figure 4.8 (i) and (j)) estimates IWU of up to 17.4 mm/month on average in the Ebro Basin for the irrigated season, and also simulates a similar amount of irrigation during the non-irrigated season, which again might be caused by noise in the SM data.

Die approbierte gedruckte Originalversion dieser Diplomarbeit ist an der TU Wien Bibliothek verfügbar
The approved original version of this thesis is available in print at TU Wien Bibliothek.
TU Bibliothek Your knowledge hub WIEN

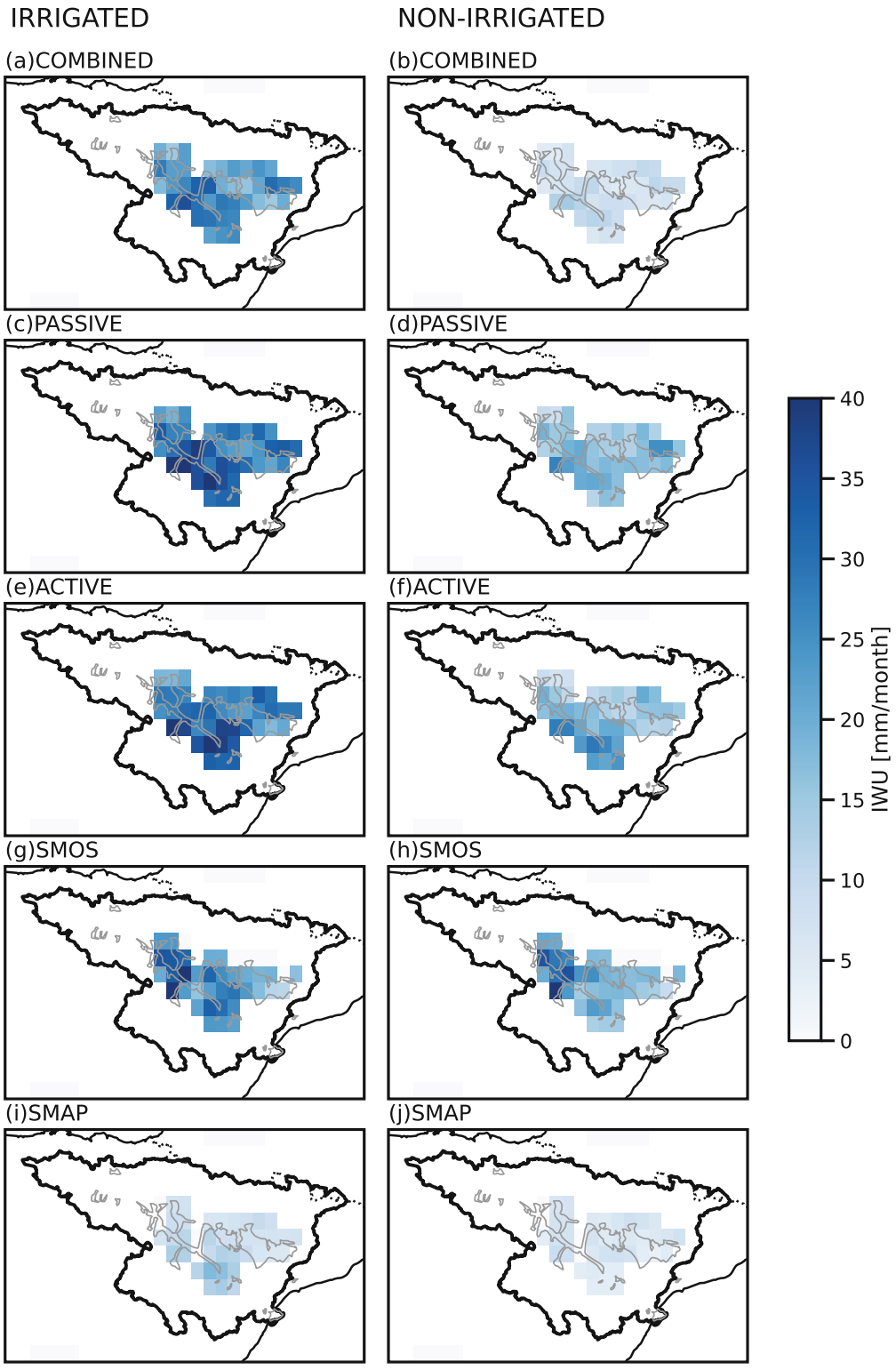

Figure 4.8: Mean monthly IWU maps for the Ebro Basin for the irrigated (March to October) and non-irrigated (November to February) seasons. ESA CCI ACTIVE (a) irrigation season and (b) non irrigation season, (c) ESA CCI COMBINED (c) irrigation and (d) non-irrigation season, ESA CCI PASSIVE (e) irrigation and (f) non-irrigation season, SMAP (g) irrigation and (h) non-irrigation season, SMOS (i) irrigation and (j) non irrigation season.

Die approbierte gedruckte Originalversion dieser Diplomarbeit ist an der TU Wien Bibliothek verfügbar
The approved original version of this thesis is available in print at TU Wien Bibliothek.
TU Bibliothek Your knowledge hub WIEN

satellite product	irrigated season in mm/month
ESA CCI COMBINED	19.8
ESA CCI PASSIVE	24.7
ESA CCI ACTIVE	24.0
SMOS	17.4
SMAP	7.1

Table 4.6: Mean monthly IWU during the irrigated season (March to October) over the Ebro Basin in mm/month.

satellite product	irrigated season in mm/month
ESA CCI COMBINED	10.7
ESA CCI PASSIVE	13.0
ESA CCI ACTIVE	9.3
SMOS	1.3
SMAP	1.9

Table 4.7: Mean monthly IWU during the irrigated season (September to April) over the Murray-Darling Basin in mm/-month.

4.4.2 Murray-Darling Basin

In comparison to the Ebro Basin, the IWU retrieval in the Murray-Darling Basin indicates a less distinct seasonal pattern. Figure 4.9 illustrates the mean monthly IWU during the irrigated and the non-irrigated seasons in the Murray-Darling Basin and Table 4.7 summarizes the mean monthly IWU averaged over the Murray-Darling Basin. SMOS and SMAP are unable to distinguish between irrigated and non-irrigated seasons, and retrieve low IWU amounts for both seasons. ESA CCI ACTIVE yields an average IWU of 9.3 mm/month during the irrigation season and lower IWU during the rest of the year. The ESA CCI COMBINED and ESA CCI PASSIVE datasets are able to differentiate between the two seasons. The retrieved IWU values during the irrigated period are on average 10.7 mm/month for the ESA CCI COMBINED product and 13.0 mm/month for the ESA CCI PASSIVE product.

Die approbierte gedruckte Originalversion dieser Diplomarbeit ist an der TU Wien Bibliothek verfügbar
The approved original version of this thesis is available in print at TU Wien Bibliothek.

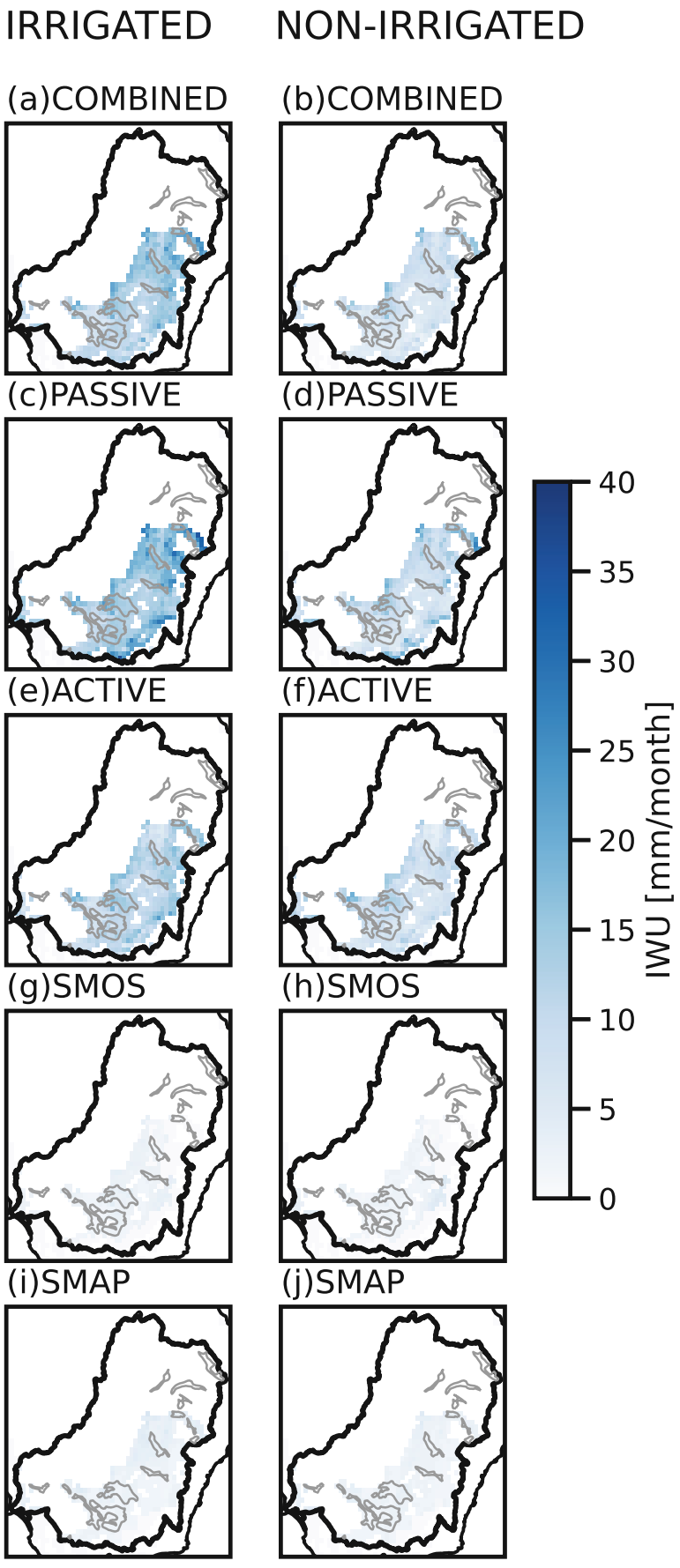

Figure 4.9: Mean monthly IWU for the Murray Basin for the irrigated (September to April) and non-irrigated (Mai to August) seasons. ESA CCI COMBINED (a) irrigation season and (b) non-irrigated season, (c) ESA CCI PASSIVE (c) irrigation and (d) non-irrigation season, ESA CCI ACTIVE (e) irrigation and (f) non-irrigation season, SMAP (g) irrigation and (h) non-irrigation season, SMOS (i) irrigation and (j) non-irrigation season.

Die approbierte gedruckte Originalversion dieser Diplomarbeit ist an der TU Wien Bibliothek verfügbar
The approved original version of this thesis is available in print at TU Wien Bibliothek.
TU Bibliothek Your knowledge hub WIEN

4.5 Evaluation using in situ irrigation data

4.5.1 Time series analysis

In this subsection, simulated irrigation is compared to in situ irrigation data in several districts in the Ebro Basin and the Murray-Darling Basin. The non-irrigated season is masked, as we know that no irrigation is applied during this period.

Ebro Basin irrigation districts

Figure 4.10 shows the time series of simulated irrigation (blue line) and measured in situ irrigation (gray) over the averaged four irrigation districts in the Ebro Basin for the period 2008 to 2022 for the five SM satellite products. The metrics bias, RMSD, and the Pearson correlation coefficient (R) are shown above the different subplots. It should be noted that the metrics were calculated over the whole simulated period, which differs between the satellite products.

The ESA CCI COMBINED product demonstrates the highest correlation (R=0.75), and the lowest RMSD (22.84 mm/month) between the in situ and the simulated IWU time series (see Table 4.8). ESA CCI PASSIVE product performs slightly below that of the ESA CCI COMBINED product with a Pearson correlation coefficient of R=0.62 and an RMSD of 27.27 mm/month. However, the picture is reversed for the bias, where ESA CCI PASSIVE (bias=-4.24 mm/month) outperforms ESA CCI COMBINED (bias=-8.07 mm/month). The SMAP and the SMOS products yield correlation coefficients of R=0.55 and R=0.58, respectively, RMSD values of 33.66 mm/month and 30.38 mm/month, and bias values of -22.47 mm/month and -16.94 mm/month. The ESA CCI ACTIVE product exhibits the poorest agreement between in situ and simulated IWU in terms of the correlation (R=0.49). Although showing a small bias (-6.49 mm/month), the RMSD value of the ESA CCI ACTIVE product is the second highest for the Ebro Basin (RMSD=32.27 mm/month).

satellite	simulated-period	BIAS $\frac{mm}{month}$	RMSD $\frac{mm}{month}$	R [-]
ESA CCI COMBINED	2008-2022	-8.07	**22.84**	**0.75**
ESA CCI PASSIVE	2008-2022	**-4.24**	27.27	0.62
ESA CCI ACTIVE	2008-2022	-6.49	32.27	0.49
SMOS	2010-2022	-16.94	30.38	0.58
SMAP	2015-2022	-22.47	33.66	0.55

Table 4.8: Metrics computed between in situ and simulated IWU in the Ebro Basin. The numbers in bold indicate the satellite with the best performance for that metric.

Murray-Darling Basin irrigation districts

Figures 4.11 to 4.14 shows the irrigation time series for the subbasins Coleambally, Murray Mulwala, Murray Wakool, and Murrumbidgee within the Murray-Darling Basin. The metrics are summarized in Tables 4.9 and 4.10.

In the Coleambally irrigation district (Figure 4.11 and Table 4.10), the ESA CCI ACTIVE and SMAP datasets show the highest performances

Die approbierte gedruckte Originalversion dieser Diplomarbeit ist an der TU Wien Bibliothek verfügbar
The approved original version of this thesis is available in print at TU Wien Bibliothek.
TU Bibliothek Your knowledge hub WIEN

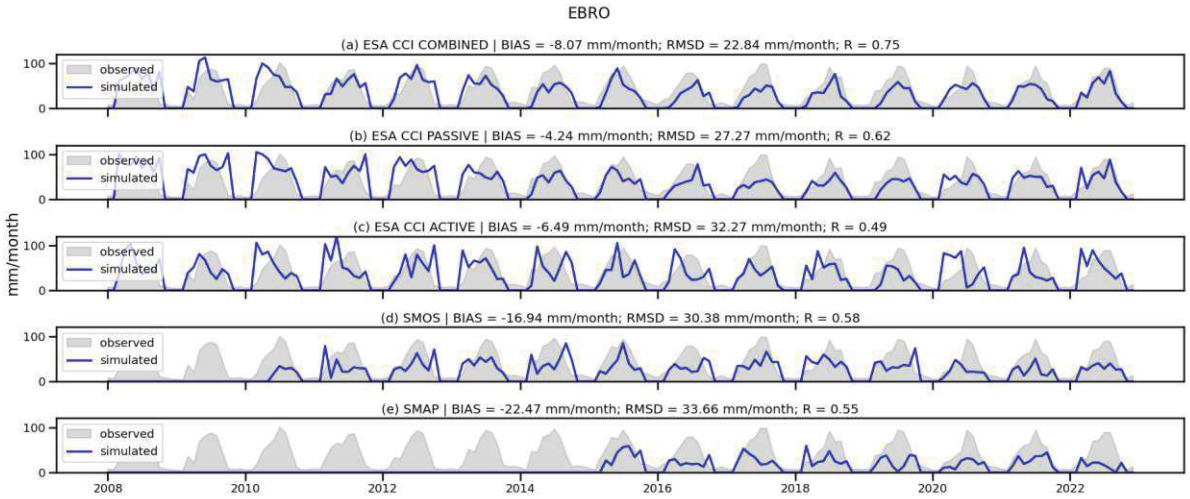

Figure 4.10: Comparison of retrieved irrigation time series with in situ data in the Ebro Basin. (a) ESA CCI COMBINED for the period 2008 to 2022, (b) ESA CCI PASSIVE for the period 2008 to 2022, (c) ESA CCI ACTIVE for the period 2008 to 2022, (d) SMOS for the period 2010 to 2022 and (e) SMAP for the period 2015 to 2022.

with R values of 0.45 and 0.44, respectively, and RMSD values of 29.88 mm/month and 18.82 mm/month.

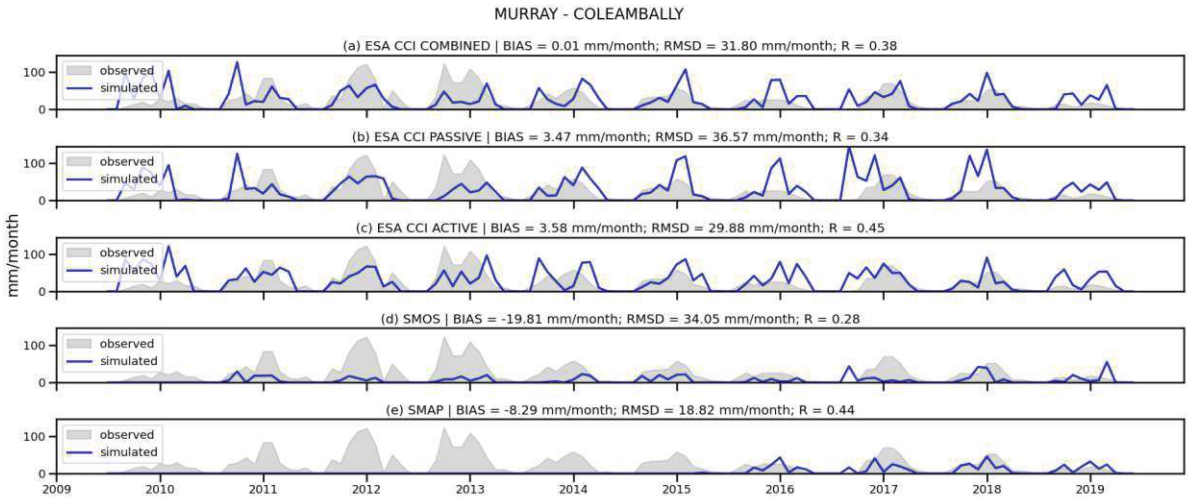

Figure 4.11: Comparison of retrieved irrigation time series with in situ data in the Coleambally Basin in Australia. (a) ESA CCI COMBINED for the period 2009 to 2019, (b) ESA CCI PASSIVE for the period 2009 to 2019, (c) ESA CCI ACTIVE for the period 2009 to 2019, (d) SMOS for the period 2010 to 2019 and (e) SMAP for the period 2015 to 2019.

In the Murray Wakool irrigation district (Figure 4.12 and Table 4.9), ESA CCI PASSIVE retrieves the irrigation dynamics best with a Pearson correlation coefficient of R=0.38. ESA CCI COMBINED (R=0.34) and ESA CCI ACTIVE (R=0.32) show a similar performance in terms of R. However, ESA CCI COMBINED (bias=5.99 mm/month, RMSD=21.77 mm/month) and ESA CCI ACTIVE (bias=5.27 mm/month, RMSD=20.79 mm/month) quantitatively retrieve IWU better compared to the ESA CCI PASSIVE product (bias= 11.85 mm/month, RMSD=27.43). SMOS (bias=-6.5 mm/month, RMSD = 14.51 mm/month) and SMAP (bias=-2.01 mm/month, RMSD=7.18 mm/month) outperform the ESA CCI products in terms of bias and RMSD, but show smaller correlation values (R=0.21 and R=0.26, respectively). Overall, ESA CCI ACTIVE performs best in the Murray Wakool district.

Die approbierte gedruckte Originalversion dieser Diplomarbeit ist an der TU Wien Bibliothek verfügbar
The approved original version of this thesis is available in print at TU Wien Bibliothek.
TU Bibliothek Your knowledge hub WIEN

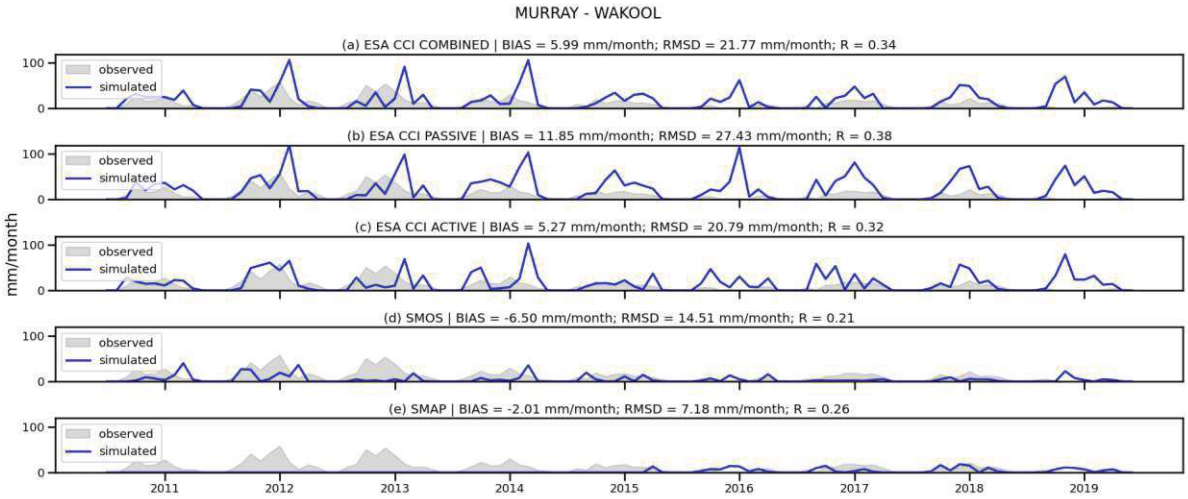

Figure 4.12: Comparison of retrieved irrigation time series with in situ data in the Murray Wakool Basin in Australia. (a) ESA CCI COMBINED for the period 2010 to 2019, (b) ESA CCI PASSIVE for the period 2010 to 2019, (c) ESA CCI ACTIVE for the period 2010 to 2019, (d) SMOS for the period 2010 to 2019 and (e) SMAP for the period 2015 to 2019.

In the Murray Mulwala district (Figure 4.13 and Table 4.10), the ESA CCI products show the best Pearson correlation values ($R_{COMBINED} = 0.45$, $R_{PASSIVE} = 0.44$, and $R_{ACTIVE} = 0.43$) compared to SMOS ($R = 0.23$) and SMAP ($R = 0.38$). While the ESA CCI products overestimate irrigation, which is indicated by a positive bias, SMOS (bias=-6.35 mm/month) and SMAP (bias=-5.70 mm/month) underestimate irrigation. Overall, ESA CCI ACTIVE (bias = 3.19 mm/month) shows the smallest absolute bias and SMAP the smallest RMSD value (RMSD= 11.35 mm/month).

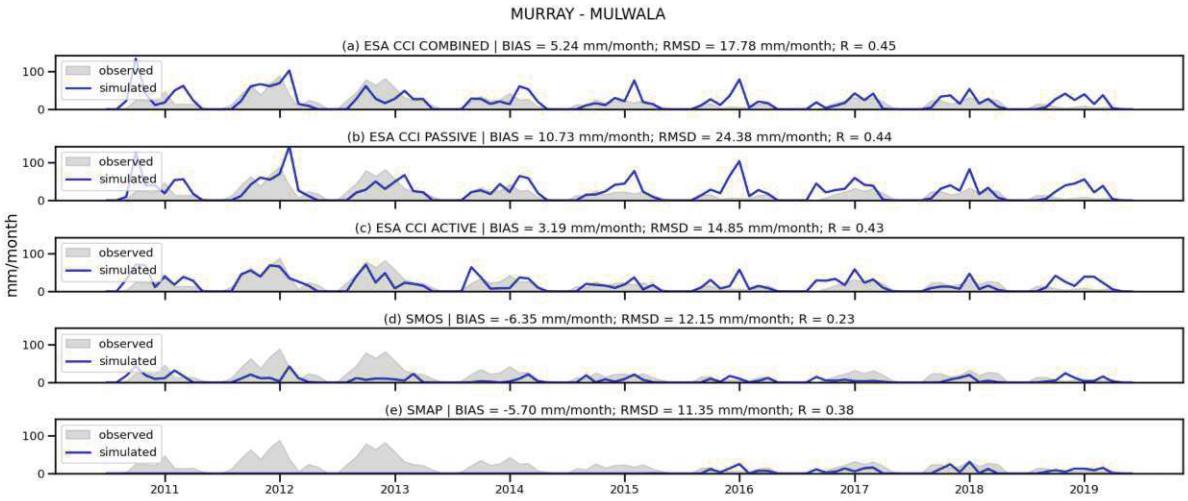

Figure 4.13: Comparison of retrieved irrigation time series with in situ data in the Murray Mulwala Basin in Australia. (a) ESA CCI COMBINED for the period 2010 to 2019, (b) ESA CCI PASSIVE for the period 2010 to 2019, (c) ESA CCI ACTIVE for the period 2010 to 2019, (d) SMOS for the period 2010 to 2019 and (e) SMAP for the period 2015 to 2019.

The ESA CCI COMBINED and ESA CCI PASSIVE products perform best in the Murrumbidgee Basin (Figure 4.14 and Table 4.10), reaching the highest Pearson correlation values of $R_{COMBINED} = 0.61$ and $R_{PASSIVE} = 0.64$, while showing the lowest RMSD values ($RMSD_{COMBINED} = 16.70 mm/month$ and $RMSD_{PASSIVE} = 19.70 mm/month$) in this sub-basin.

SMAP Pearson correlation coefficient are computed with data from 2015 onwards and from 2010 onwards for SMOS. However, in situ IWU during the years 2011 to 2014 was approximately twice as high compared to subsequent years. Consequently, the calculated RMSD is significantly influenced by the time span of available in situ irrigation data.

Die approbierte gedruckte Originalversion dieser Diplomarbeit ist an der TU Wien Bibliothek verfügbar
The approved original version of this thesis is available in print at TU Wien Bibliothek.
TU Bibliothek Your knowledge hub WIEN

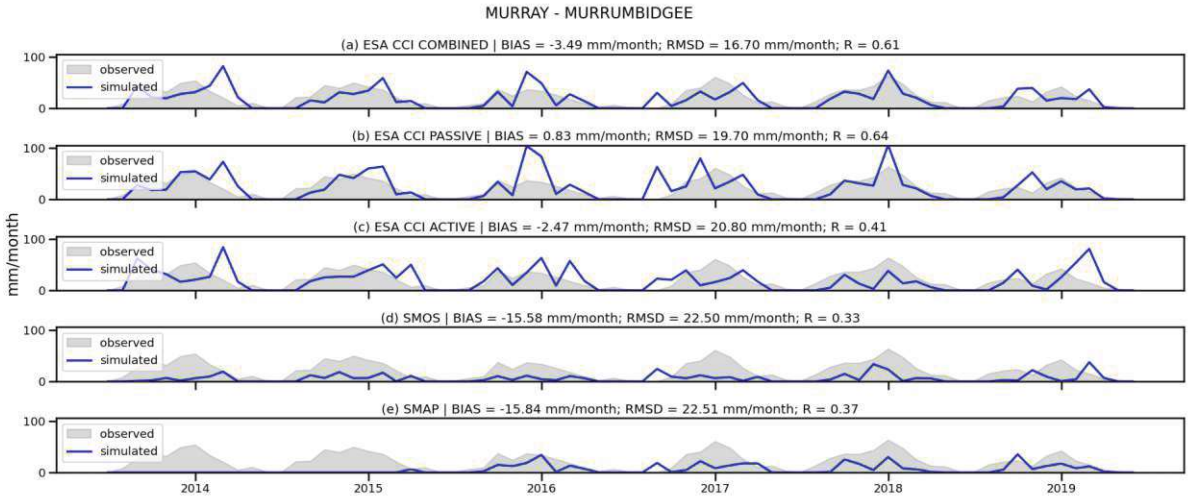

Figure 4.14: Comparison of retrieved irrigation time series with in situ data in the Murrumbidgee Basin in Australia. (a) ESA CCI COMBINED for the period 2013 to 2019, (b) ESA CCI PASSIVE for the period 2013 to 2019, (c) ESA CCI ACTIVE for the period 2013 to 2019, (d) SMOS for the period 2013 to 2019 and (e) SMAP for the period 2015 to 2019.

In the Murray Wakool, Murray Mulwala, and Coleambally districts, ESA CCI ACTIVE shows the strongest performance, while ESA CCI PASSIVE and ESA CCI COMBINED achieve the best results in the Murrumbidgee district. However, when evaluating the overall best-performing product, ESA CCI COMBINED emerges as the top choice due to its consistent performance across all regions, striking a balance between low RMSD and strong correlation.

Table 4.9: Metrics between in situ and simulated IWU in the Murray-Darling Basin. The numbers in bold indicate the satellite with the best performance for that metric.

		Coleambally			Murray Wakool		
satellite	simulated-period	BIAS $\frac{mm}{month}$	RMSD $\frac{mm}{month}$	R [-]	BIAS $\frac{mm}{month}$	RMSD $\frac{mm}{month}$	R [-]
ESA CCI COMBINED	2009/2010-2019	**0.01**	31.80	0.38	5.99	21.77	0.34
ESA CCI PASSIVE	2009/2010-2019	3.47	36.57	0.34	11.85	27.43	**0.38**
ESA CCI ACTIVE	2009/2010-2019	3.58	29.88	**0.45**	5.27	20.79	0.32
SMOS	2010-2019	-19.81	34.05	0.28	-6.50	14.51	0.21
SMAP	2015-2019	-8.29	**18.82**	0.44	**-2.01**	**7.18**	0.26

Die approbierte gedruckte Originalversion dieser Diplomarbeit ist an der TU Wien Bibliothek verfügbar
The approved original version of this thesis is available in print at TU Wien Bibliothek.
TU Bibliothek Your knowledge hub WIEN

Table 4.10: Metrics between in situ and simulated IWU in the Murray-Darling Basin.

		Murray Mulwala			Murrumbidgee		
satellite	validation-period	BIAS $\frac{mm}{month}$	RMSD $\frac{mm}{month}$	R [-]	BIAS $\frac{mm}{month}$	RMSD $\frac{mm}{month}$	R [-]
ESA CCI COMBINED	2010/2013-2019	5.24	17.78	**0.45**	-3.49	**16.70**	0.61
ESA CCI PASSIVE	2010/2013-2019	10.73	24.38	0.44	**0.83**	19.70	**0.64**
ESA CCI ACTIVE	2010/2013-2019	**3.19**	14.85	0.43	-2.47	20.80	0.41
SMOS	2010/2013-2019	-6.35	12.15	0.23	-15.58	22.50	0.33
SMAP	2015-2019	-5.70	**11.35**	0.38	-15.84	22.51	0.37

4.5.2 Scatter plots

Figures 4.15 to 4.17 show scatterplots of monthly simulated (x-axis) and in situ (y-axis) IWU along with the Pearson correlation coefficient R, the bias and the RMSD for the five SM products, computed only for the irrigated seasons. [1] If the points cluster above the line of equality (dotted line), the simulated IWU is underestimated. Conversely, if the points cluster below the line of equality, the simulated IWU is overestimated.

1: Data points lying outside of the irrigated period are masked and also metrics are computed only on the irrigated period. Hence, correlations are expected to be lower, RMSD, and bias to be higher, compared to the metrics computed in Section 4.5.1, where the whole period was considered for the computation of the metrics.

Bias values close to zero indicate that dots are evenly distributed on both sides of the equality line. Meanwhile, dots located inside the gray area indicate little under- and overestimation leading to a small RMSD value. The Pearson correlation coefficient indicates if the simulated and the in situ IWU have a linear relationship or not. Values close to 1 indicate a strong positive correlation, whereas negative values indicate a negative correlation. R values close to 0 represent datasets with a weak correlation.

Ebro Basin irrigation districts

Figure 4.15 illustrates that the ESA CCI products over- and underestimate IWU amounts over the irrigation districts located in the Ebro Basin. This is indicated by the wide spread of the data points lying outside the gray area and further confirmed by the RMSD values of 26.99 mm/month, 32.63 mm/month, and 38.91 mm/month for ESA CCI COMBINED, ESA CCI PASSIVE and ESA CCI ACTIVE, respectively. Values situated within the gray marked area exhibit a relative error of less than 30 %.

In terms of irrigation dynamics, the ESA CCI COMBINED product demonstrates the highest correlation, with R=0.45. Meanwhile, ESA CCI PASSIVE, SMOS, and SMAP exhibit positive correlation values of R=0.11, R=0.05, and R=0.05, respectively. ESA CCI ACTIVE, on the other hand, shows a slightly negative correlation of R=-0.09. A major difference between the ESA CCI products and SMOS and SMAP is found when looking at the bias value. The bias values of -7.28 mm/month, -1.50 mm/month, and -5.18 mm/month for the ESA CCI COMBINED, ESA CCI PASSIVE, and ESA CCI ACTIVE products, respectively, indicate that these products show deviations that are relatively balanced around the equality line. SMOS and SMAP, however, show systematic underestimations indicated by a bias value of -20.03 mm/month and -28.79 mm/month, respectively.

Die approbierte gedruckte Originalversion dieser Diplomarbeit ist an der TU Wien Bibliothek verfügbar
The approved original version of this thesis is available in print at TU Wien Bibliothek.
TU Bibliothek Your knowledge hub WIEN

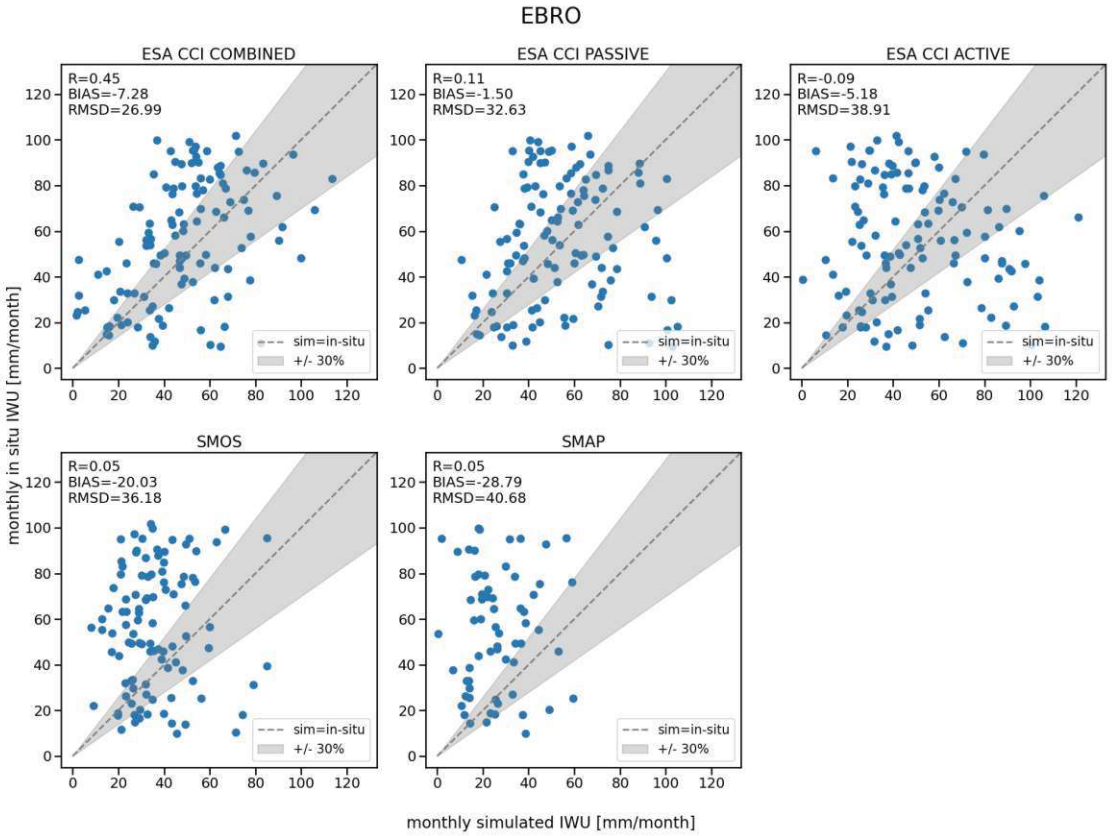

Figure 4.15: Comparison of simulated and in situ IWU in the Ebro Basin.

Murray-Darling Basin irrigation districts

Figures 4.16 to 4.19 show scatterplots of monthly simulated (x-axis) and in situ (y-axis) IWU for the four irrigation districts in the Murray-Darling Basin.

In the Mulwala subbasin, the ESA CCI ACTIVE product yields the best correlation of R=0.46 as well as the lowest absolute bias (bias=2.32 mm/month), indicating a small overestimation on average. In addition, the RMSD yields 19.81 mm/month. The ESA CCI COMBINED product provides a similar picture, as it shows a weaker positive correlation (R=0.30), but the bias of 6.12 mm/month still indicates only a slight overestimation. However, the RMSD of 26.60 mm/month of the ESA CCI COMBINED product indicates that significant over- and underestimations are observed. SMAP shows a similarly strong correlation of R=0.29, with a bias of -4.30 mm/month and an RMSD of 11.00 mm/month, suggesting that IWU is more accurately retrieved compared to the other products. However, it has to be considered, that the validation period for SMAP is shorter compared to the other satellite products and IWU amounts vary within the analyzed period. ESA CCI PASSIVE has a weak positive correlation (R=0.19), an acceptable bias (11.67 mm/month), and RMSD (31.75 mm/month). Simulated IWU retrieved from SMOS does not correlate with in situ IWU (R=0.02). Overall, for the Murray Mulwala district ESA CCI ACTIVE performs best.

In the Murray Wakool district, as none of the IWU datasets shows high correlations ($R_{COMBINED} = 0.09$, $R_{PASSIVE} = 0.11$, $R_{ACTIVE} = 0.06$, $R_{SMOS} = -0.02$ and $R_{SMAP} = 0.16$). Bias values vary between -0.02

Die approbierte gedruckte Originalversion dieser Diplomarbeit ist an der TU Wien Bibliothek verfügbar
The approved original version of this thesis is available in print at TU Wien Bibliothek.
TU Bibliothek Your knowledge hub WIEN

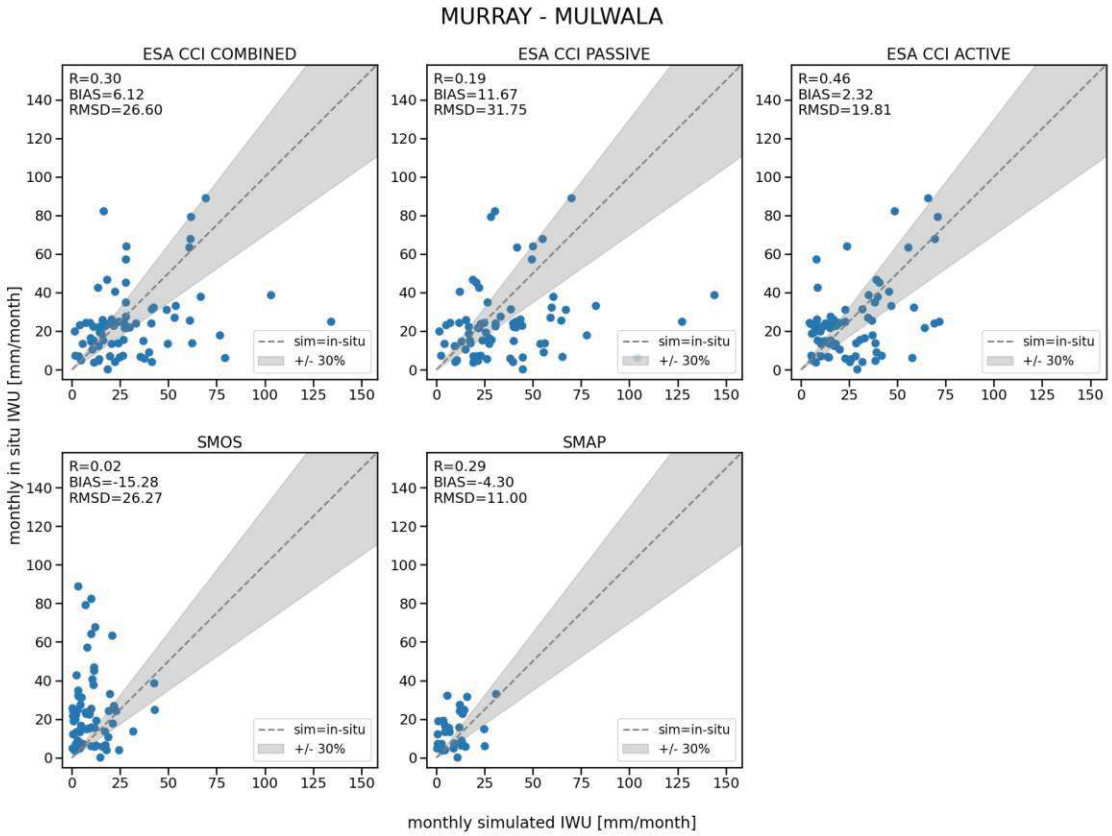

Figure 4.16: Comparison of simulated and in situ IWU in the Murray Mulwala Basin.

mm/month for SMAP and 18.94 mm/month for ESA CCI PASSIVE and RMSD values reach from 7.11 mm/month for SMAP to 33.47 mm/month for ESA CCI PASSIVE. SMAP demonstrates the best performance in the Murray Wakool district. However, when considering longer time series, the ESA CCI COMBINED product offers the best trade-off.

The Coleambally district in the Murray-Darling Basin presents a similarly low correlation for most of the satellite products ($R_{COMBINED}$ = 0.08, $R_{PASSIVE}$ = 0.04, R_{ACTIVE} = 0.13 and R_{SMOS} = −0.10). Only SMAP shows a small positive correlation (R_{SMAP} = 0.29). However, RMSD values are even higher compared to the Murray Wakool district reaching values up to 44.80 mm/month for ESA CCI PASSIVE. In terms of metrics, SMAP performs best in the Coleambally district. Out of the three ESA CCI products, ESA CCI ACTIVE performs best in the Coleambally district.

In the Murrumbidgee district, ESA CCI PASSIVE shows the strongest correlation between simulated and in situ IWU measurements, with a moderate positive correlation (R=0.42). ESA CCI COMBINED and SMAP also display positive correlations (R=0.32 and R=0.35, respectively). In contrast, ESA CCI ACTIVE and SMOS exhibit negligible correlations with simulated IWU (R=-0.04 and R=-0.08, respectively), suggesting limited alignment with in situ observations. Notably, ESA CCI ACTIVE demonstrates the smallest absolute bias (BIAS=-0.91 mm/month), indicating a balanced representation of over- and underestimation across the simulation period. Meanwhile, ESA CCI COMBINED achieves the lowest RMSD (RMSD=19.65 mm/month) among the five products, highlighting its superior quantitative alignment with in situ IWU measurements. The

Die approbierte gedruckte Originalversion dieser Diplomarbeit ist an der TU Wien Bibliothek verfügbar
The approved original version of this thesis is available in print at TU Wien Bibliothek.
TU Bibliothek Your knowledge hub WIEN

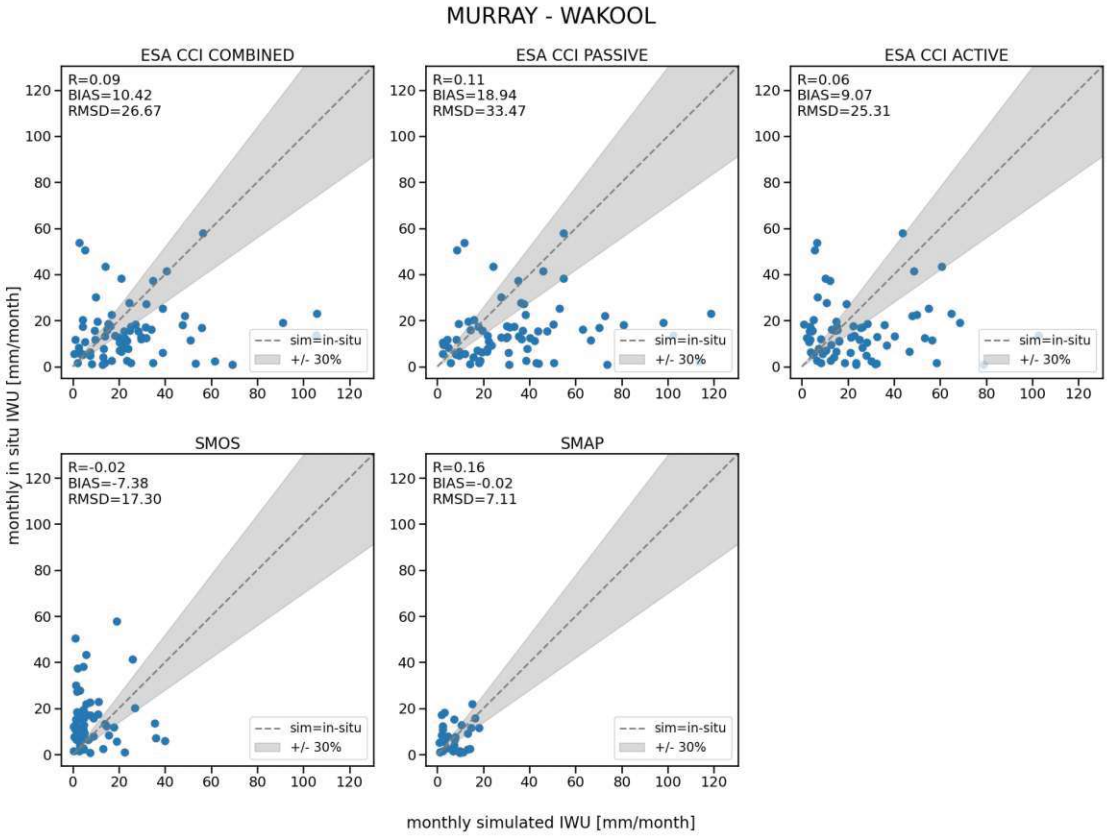

Figure 4.17: Comparison of simulated and in situ IWU in the Murray Wakool Basin.

ESA CCI PASSIVE performs best in the Murrumbidgee district, due to the high correlation.

Overall, the ESA CCI ACTIVE product performs best in specific subbasins of the Murray-Darling Basin. However, if a single product were to be chosen, the ESA CCI COMBINED product would be the preferred option due to its consistent performance across all regions, striking a balance between low RMSD and strong correlation.

Die approbierte gedruckte Originalversion dieser Diplomarbeit ist an der TU Wien Bibliothek verfügbar
The approved original version of this thesis is available in print at TU Wien Bibliothek.

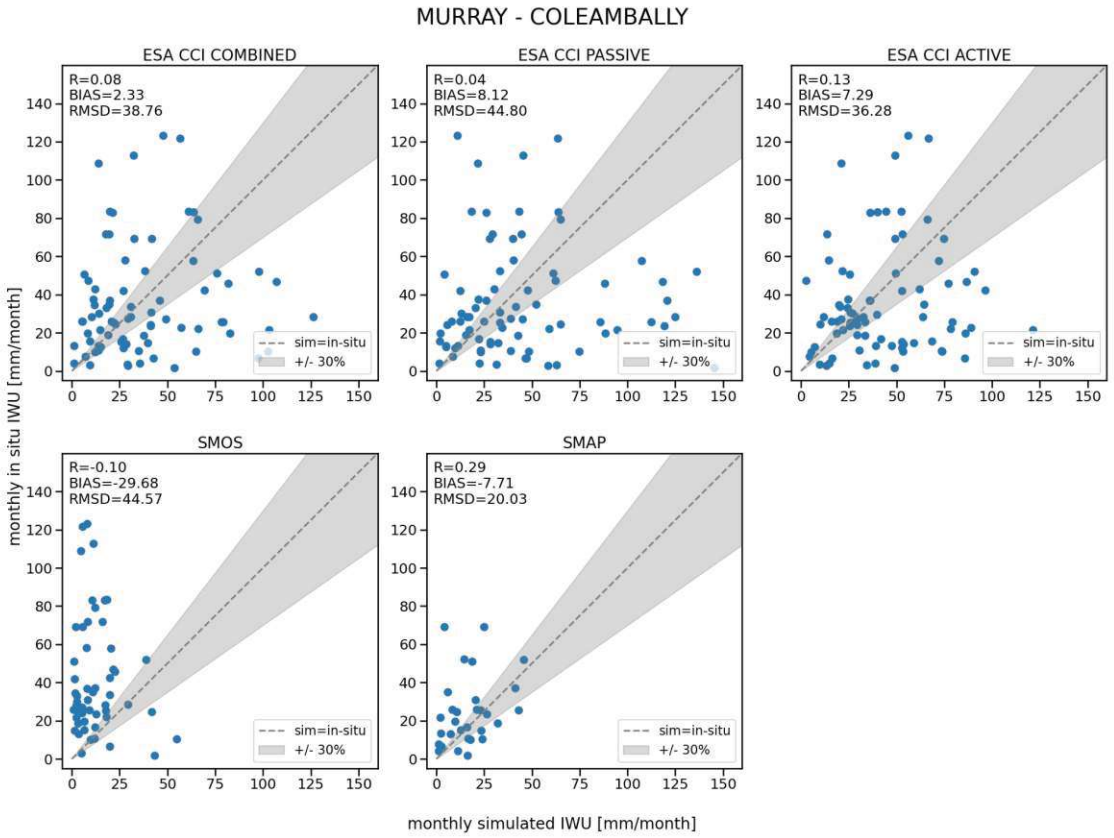

Figure 4.18: Comparison of simulated and in situ IWU in the Coleambally Basin.

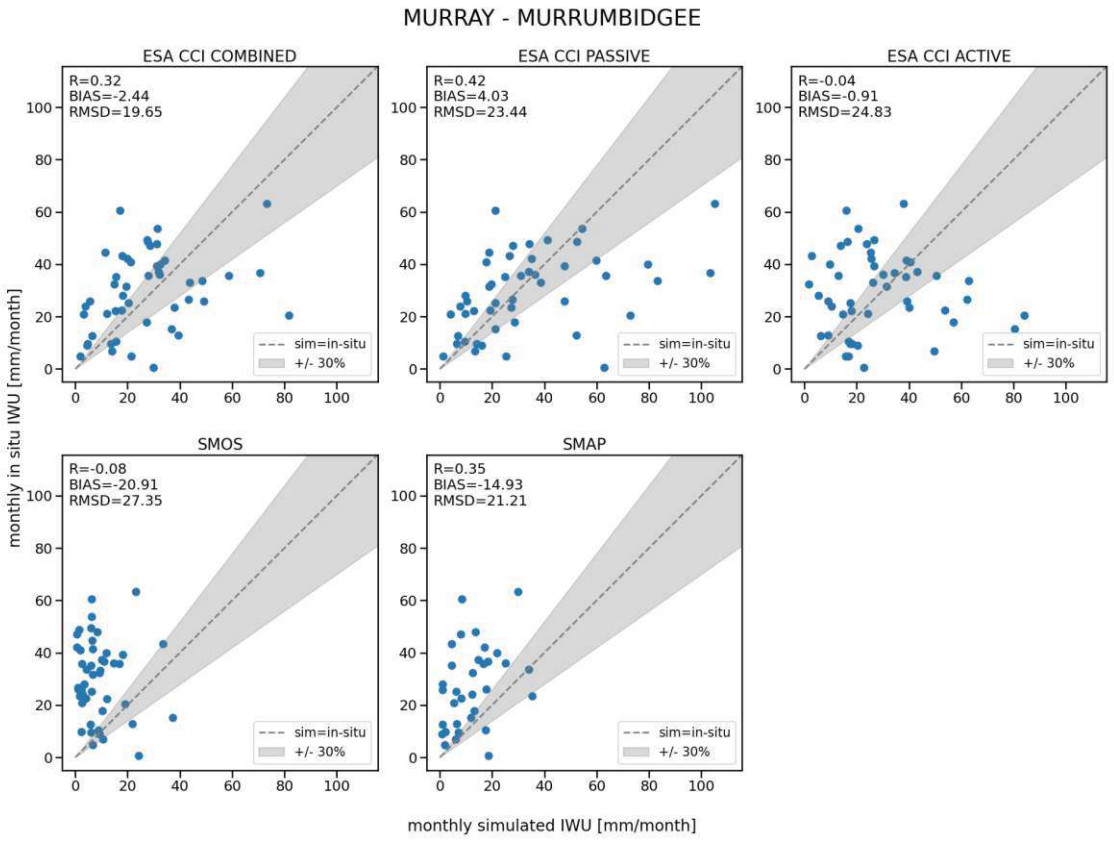

Figure 4.19: Comparison of simulated and in situ IWU in the Murrumbidgee Basin.

Die approbierte gedruckte Originalversion dieser Diplomarbeit ist an der TU Wien Bibliothek verfügbar
The approved original version of this thesis is available in print at TU Wien Bibliothek.
TU Bibliothek Your knowledge hub WIEN

Die approbierte gedruckte Originalversion dieser Diplomarbeit ist an der TU Wien Bibliothek verfügbar
The approved original version of this thesis is available in print at TU Wien Bibliothek.

5 Discussion

In the Murray-Darling Basin, the observed decrease in simulated and in situ irrigation over time can be attributed to increasingly larger irrigation areas (see Section 3.5). As a result, irrigation volumes are spread over a larger area and even though irrigation volumes at the district scale vary little from one year to the next, water heights per unit area are decreasing over time. During the 2015/2016 irrigation season, in situ irrigation is particularly low, due to restrictions in IWU caused by droughts during this period [40]. The lower irrigation values are not reflected in the simulated IWU, leading to overestimated irrigation. This overestimation may originate from noisy SM data not being able to reflect the low SM values. Furthermore, the limited availability of SMAP data, starting only in 2015, complicates the evaluation of whether the observed good metrics genuinely reflect strong model performance or are influenced by dataset constraints.

[40]: Bretreger et al. (2020), 'Monitoring irrigation using landsat observations and climate data over regional scales in the Murray-Darling Basin'

The performance of satellite-SM-based IWU products varies across the subbasins in the Murray-Darling Basin (see Tables 4.9 and 4.10). Those differences in performance might arise from the different crop types, precipitation amounts, or irrigation densities varying between the districts [40]. ESA CCI ACTIVE performs best in the Murray Wakool, Murray Mulwala, and Coleambally districts, while ESA CCI PASSIVE yields the best results in the Murrumbidgee district. However, when considering overall performance, ESA CCI COMBINED emerges as the most reliable product, consistently balancing low RMSD and strong correlation across all regions.

[40]: Bretreger et al. (2020), 'Monitoring irrigation using landsat observations and climate data over regional scales in the Murray-Darling Basin'

The comparison of the retrieved IWU with the in situ IWU in the Ebro basin, as shown in Figure 4.10 and Table 4.8, demonstrates the better performance of the ESA CCI SM products when compared to SMOS and SMAP to retrieve irrigation. ESA CCI COMBINED shows the best performance, with the highest correlation (R=0.75) and lowest RMSD (22.84 mm/month) in the Ebro Basin. This is in line with the finding of Zohaib et Choi (2020) [34], who compared country-aggregated IWU estimations using SM Delta with observed IWU at the global scale, and found that ESA CCI COMBINED (R=0.80) outperforms the ESA CCI PASSIVE (R=0.72) and ESA CCI ACTIVE (R=0.77) product. One of the reasons for the better performance of the ESA CCI COMBINED product may be that it is the only one of the five products analyzed that combines measurements from active and passive sensors. As a result, ESA CCI COMBINED SM has a higher signal-to-noise ratio than ESA CCI ACTIVE and ESA CCI PASSIVE, resulting in more accurate SM data overall.

[34]: Zohaib et al. (2020), 'Satellite-based global-scale irrigation water use and its contemporary trends'

However, all five satellite products significantly underestimate the IWU in the Ebro Basin, which is indicated by the negative bias values obtained. The ESA CCI products yield the lowest absolute bias values (-8.07

Die approbierte gedruckte Originalversion dieser Diplomarbeit ist an der TU Wien Bibliothek verfügbar
The approved original version of this thesis is available in print at TU Wien Bibliothek.
TU Bibliothek Your knowledge hub WIEN

mm/month, -4.24 mm/month, and -6.49 mm/month for COMBINED, PASSIVE, and ACTIVE, respectively compared to -16.94 mm/month and -22.47 mm/month for SMOS and SMAP) and hence the lowest underestimation of the five satellite products. Especially for SMOS and SMAP, the months with higher observed in situ IWU values (June to August) are significantly underestimated. An explanation for that might be their revisit time of 3 days. Indeed, because of the low frequency, not all irrigation events are captured leading to an underestimation [27]. Furthermore, as explained in Section 3.4, irrigation events captured during a data gap between two observations further than 4 days apart, are conservatively disregarded by the implemented algorithm. The revisit time of 3 days of SMOS and SMAP makes it more probable that this exception is applied, namely, as soon as there is one observation missing due to masking of erroneous data.

The underestimations observed are in line with the results of several studies. Zaussinger et al. (2019) [25] applied the SM Delta algorithm to the CONUS using coarse-resolution SM data (ASCAT, AMSR2, and SMAP) and validated the retrieved irrigation at the state scale. Despite showing high correlations between estimated and observed IWU at the state scale, especially for SMAP (R=0.8), they found that irrigation is underestimated across all analyzed products (bias=-2.36 km^3 on average for the three products). Another study by Zohaib et Choi (2020) [34] applied the SM Delta algorithm to ESA CCI ACTIVE, ESA CCI PASSIVE, and ESA CCI COMBINED SM globally and validated the retrieved IWU at the country level. They also found that IWU is underestimated (bias=-75.5 km^3 on average for the three products). The underestimation of IWU is generally attributed to the coarse scale resolution of the SM products used and the exclusion of ET in the SM Delta approach. [26, 27] Using coarse spatial resolution SM data may lead to an underestimation of IWU, especially in small, sparsely irrigated areas. Zappa et al. (2022) [27] found that high-resolution IWU retrievals are able to detect irrigation events on the field scale, whereas it is more challenging using coarse-scale resolution data since the irrigation signal is less strong. This may lead to a significant underestimation of the irrigation amounts detected. However, high-resolution data are not available globally and on a long-term basis. Several studies used Sentinel-1-derived (Zappa et al. (2021, 2022, 2024) [26–28], Dari et al. (2023) [30]) SM products to retrieve high-resolution IWU, but for shorter periods and a limited spatial domain.

In a recent study, Zappa et al. (2024) [28] compared IWU obtained with Sentinel-1 SM data at 1 km using the SM Delta approach, the SM Inversion method, a satellite-based irrigation retrieval approach based on the inversion of the soil water balance equation (Brocca et al. (2018) [29], Dari et al. (2020), (2022), (2023) [30–32]), and a model assimilation approach based on Noah-MP (Modanesi et al. [21]), over the Ebro Basin. When comparing IWU retrieved with the SM Delta method with in situ IWU data, they found a Pearson correlation coefficient of approximately 0.65, a bias of -10 mm/month, and an ubRMSD of 24 mm/month. Their results are in line with the results of this study but do not show the

[27]: Zappa et al. (2022), 'How accurately can we retrieve irrigation timing and water amounts from (satellite) soil moisture?'

[25]: Zaussinger et al. (2019), 'Estimating irrigation water use over the contiguous United States by combining satellite and reanalysis soil moisture data'

[34]: Zohaib et al. (2020), 'Satellite-based global-scale irrigation water use and its contemporary trends'

[26]: Zappa et al. (2021), 'Detection and Quantification of Irrigation Water Amounts at 500 m Using Sentinel-1 Surface Soil Moisture'

[27]: Zappa et al. (2022), 'How accurately can we retrieve irrigation timing and water amounts from (satellite) soil moisture?'

[26]: Zappa et al. (2021), 'Detection and Quantification of Irrigation Water Amounts at 500 m Using Sentinel-1 Surface Soil Moisture'

[27]: Zappa et al. (2022), 'How accurately can we retrieve irrigation timing and water amounts from (satellite) soil moisture?'

[28]: Zappa et al. (2024), 'Benefits and pitfalls of irrigation timing and water amounts derived from satellite soil moisture'

[30]: Dari et al. (2023), 'Regional data sets of high-resolution (1 and 6 km) irrigation estimates from space'

[29]: Brocca et al. (2015), 'Rainfall estimation from in situ soil moisture observations at several sites in Europe: an evaluation of the SM2RAIN algorithm'

[30]: Dari et al. (2023), 'Regional data sets of high-resolution (1 and 6 km) irrigation estimates from space'

[31]: Dari et al. (2022), 'Irrigation estimates from space: Implementation of different approaches to model the evapotranspiration contribution within a soil-moisture-based inversion algorithm'

[32]: Dari et al. (2020), 'Exploiting High-Resolution Remote Sensing Soil Moisture to Estimate Irrigation Water Amounts over a Mediterranean Region'

[21]: Modanesi et al. (2022), 'Challenges and benefits of quantifying irrigation through the assimilation of Sentinel-1 backscatter observations into Noah-MP'

Die approbierte gedruckte Originalversion dieser Diplomarbeit ist an der TU Wien Bibliothek verfügbar
The approved original version of this thesis is available in print at TU Wien Bibliothek.
TU Bibliothek Your knowledge hub WIEN

expected improvement due to the use of high-resolution SM data. The SM Inversion approach showed similar performances (approximately R= 0.7, bias = -8 mm/month, and ubRMSD = 22 mm/month). Those results are also comparable to those of Dari et al. (2023) [30], who applied high-resolution SM data from Sentinel 1 to the SM-based Inversion algorithm to estimate IWU over the Ebro, Po, and Murray-Darling basins. Analyzing the years 2016 to 2020, they obtained similar metrics as we did in our study in the irrigation districts of the Ebro Basin (RMSD=26 mm/month, R=0.60, and bias =-13.47 mm/month). Over the Murray-Darling Basin, their results demonstrated higher correlation coefficients (R=0.66 to R=0.84) and lower RMSD values (8.65 mm/month to 15.22 mm/month) compared to our study, where R ranged from 0.32 to 0.64 and RMSD from 14.85 mm/month to 36.57 mm/month for ESA CCI products. Notably, their analysis is limited to 2016 and 2017, reducing its representativeness for broader temporal variability. The fact that the results obtained with high-resolution SM data are as good as those we achieved with coarse-scale SM data in the Ebro Basin is a significant finding. This challenges the commonly cited argument that high resolution is necessary to avoid underestimation and the quality of the estimates obtained with high-resolution SM data.

[30]: Dari et al. (2023), 'Regional data sets of high-resolution (1 and 6 km) irrigation estimates from space'

Underestimation of IWU might be due to the fact that we do not take into account the difference in ET between satellite observations (irrigated pixel) and model observations (non-irrigated pixel), assuming in equation 3.9 that ET is the same between the both. Several studies (Zappa et al. (2024) [28], Kragh et al. (2024) [68] and Dari et al. (2020) [32]) showed that leaving out the information on ET could be the reason for this underestimation. The increased SM caused by irrigation leads to increased ET making the latter differ considerably between irrigated and rainfed fields. Hence, including ET is expected to reduce the underestimation of IWU. In their study, Zappa et al. (2021) [26] took into account ET in the SM Delta algorithm by adding the difference in ET between irrigated and rainfed fields to the irrigation retrieved using SM data. They found that ET contributed twice as much as SM to the estimated irrigation water level, improving irrigation estimates. Kragh et al. (2024) [68] investigated different approaches similar to the SM Delta algorithm by employing a range of techniques, including SM alone, ET alone, and a joint approach, and concluded that the joint approach is the most effective method for retrieving irrigation when compared to benchmark data. Moreover, several studies by Brocca et al. (2018) [29] and Dari et al. (2020, 2022a, 2023) [30–32] used ET in the SM-based inversion algorithm.

[28]: Zappa et al. (2024), 'Benefits and pitfalls of irrigation timing and water amounts derived from satellite soil moisture'

[68]: Kragh et al. (2024), 'An intercomparison of approaches and frameworks to quantify irrigation from satellite data'

[32]: Dari et al. (2020), 'Exploiting High-Resolution Remote Sensing Soil Moisture to Estimate Irrigation Water Amounts over a Mediterranean Region'

[26]: Zappa et al. (2021), 'Detection and Quantification of Irrigation Water Amounts at 500 m Using Sentinel-1 Surface Soil Moisture'

[68]: Kragh et al. (2024), 'An intercomparison of approaches and frameworks to quantify irrigation from satellite data'

[29]: Brocca et al. (2015), 'Rainfall estimation from in situ soil moisture observations at several sites in Europe: an evaluation of the SM2RAIN algorithm'

[30]: Dari et al. (2023), 'Regional data sets of high-resolution (1 and 6 km) irrigation estimates from space'

[31]: Dari et al. (2022), 'Irrigation estimates from space: Implementation of different approaches to model the evapotranspiration contribution within a soil-moisture-based inversion algorithm'

[32]: Dari et al. (2020), 'Exploiting High-Resolution Remote Sensing Soil Moisture to Estimate Irrigation Water Amounts over a Mediterranean Region'

Future research should address the limitations highlighted in this study by focusing on improving the temporal resolution of SM datasets in future missions to capture irrigation events better. Moreover, exploring the integration of additional hydrological variables, such as ET data, could help refine IWU estimates and reduce underestimation. Expanding the availability of in situ irrigation data, such as the CONUS Irrigation and Water Management Survey dataset [69], is also crucial for better validating our approach and confirming the results obtained for the

[69]: (2019), '2018 Irrigation and Water Management Survey'

Die approbierte gedruckte Originalversion dieser Diplomarbeit ist an der TU Wien Bibliothek verfügbar
The approved original version of this thesis is available in print at TU Wien Bibliothek.
TU Bibliothek Your knowledge hub WIEN

Ebro and Murray-Darling basins. Finally, extending these analyses to other regions and incorporating longer validation periods could provide valuable insights into the adaptability and consistency of these methods across varying climatic and agricultural conditions.

Die approbierte gedruckte Originalversion dieser Diplomarbeit ist an der TU Wien Bibliothek verfügbar
The approved original version of this thesis is available in print at TU Wien Bibliothek.
TU Bibliothek Your knowledge hub WIEN

Conclusion 6

This thesis demonstrates the potential of the SM Delta method for estimating long-term IWU using five coarse-resolution satellite-derived SM products. By applying the method to long-term datasets, this study offers a novel contribution to the field. The SM Delta approach [25] was evaluated in the Ebro and Murray-Darling basins using in situ data to assess its ability to capture long-term irrigation dynamics with coarse-scale SM data.

[25]: Zaussinger et al. (2019), 'Estimating irrigation water use over the contiguous United States by combining satellite and reanalysis soil moisture data'

Spatial statistical analysis of the differences between the satellite SM datasets and the model dataset showed that the three ESA CCI products demonstrate clear distinctions between irrigated and non-irrigated seasons, making them strong candidates for IWU retrieval. Furthermore, the ESA CCI products, with near-daily observations, outperform SMOS and SMAP in terms of their observation frequency.

When using the three ESA CCI SM datasets, the SM Delta method was able to reproduce quite well the irrigation dynamics related to the irrigated and rainfed season, which was not the case using SMAP and SMOS SM data. The distinction between irrigated and non-irrigated seasons was less apparent in the Murray-Darling Basin for all datasets.

Validation with in situ data showed that the ESA CCI COMBINED (R=0.75, bias=-8.07 mm/month and RMSD=22.84 mm/month) and ESA CCI PASSIVE (R=0.62, bias=-4.24 mm/month and RMSD=27.27 mm/month) products best captured the irrigation dynamics in the Ebro Basi among the five products. In the Murray-Darling Basin, ESA CCI COMBINED is identified as the most reliable product, demonstrating a consistent balance of low RMSD (22.01 mm/month on average) and strong correlation (R=0.45 on average) across all regions.

The study identified two key findings: first, IWU retrieval using coarse spatial resolution SM data performs comparably to high-resolution methods over the Ebro Basin, challenging the assumption that higher resolution always yields better results. Second, the omission of ET in the algorithm is a critical limitation. Since irrigation increases ET, excluding ET may lead to underestimations by not fully accounting for its role in the water balance. Future improvements should focus on integrating ET to enhance accuracy.

In conclusion, the SM Delta method shows strong potential for long-term IWU retrieval, particularly with high-frequency datasets like ESA CCI COMBINED and ESA CCI PASSIVE. Incorporating ET could improve IWU estimates. These datasets mark a significant step toward integrating anthropogenic impacts into climate models and improving water resource management.

Die approbierte gedruckte Originalversion dieser Diplomarbeit ist an der TU Wien Bibliothek verfügbar
The approved original version of this thesis is available in print at TU Wien Bibliothek.
TU Bibliothek Your knowledge hub WIEN

Die approbierte gedruckte Originalversion dieser Diplomarbeit ist an der TU Wien Bibliothek verfügbar
The approved original version of this thesis is available in print at TU Wien Bibliothek.

Bibliography

[1] Kukal, Meetpal S & Irmak, Suat. 'Irrigation-limited yield gaps: trends and variability in the United States post-1950'. In: *Environmental Research Communications* 1.6 (2019), p. 061005. DOI: 10.1088/2515-7620/ab2aee (cited on page 1).

[2] Allan, Richard & Soden, Brian. 'Atmospheric warming and the amplification of precipitation extremes.' In: *Science* (2008). DOI: doi:10.1126/science.1160787 (cited on page 1).

[3] WWAP (UNESCO World Water Assessment Programme). *The United Nations world water development report 2019: leaving non one behind*. Paris, UNESCO, 2019 (cited on page 1).

[4] Deng, Jia; Guo, Lei; Salas, William; Ingraham, Pete; Charrier-Klobas, Jessica G.; Frolking, Steve & Li, Changsheng. 'Changes in Irrigation Practices Likely Mitigate Nitrous Oxide Emissions From California Cropland'. In: *Global Biogeochemical Cycles* 32.10 (2018), pp. 1514–1527. DOI: https://doi.org/10.1029/2018GB005961 (cited on page 1).

[5] Famiglietti, J. 'The global groundwater crisis'. In: *Nature Climate Change* 4 (2014), pp. 945–948. DOI: https://doi.org/10.1038/nclimate2425 (cited on page 1).

[6] Pokhrel, Yadu N.; Hanasaki, Naota; Wada, Yoshihide & Kim, Hyungjun. 'Recent progresses in incorporating human land–water management into global land surface models toward their integration into Earth system models'. In: *WIREs Water* 3.4 (2016), pp. 548–574. DOI: https://doi.org/10.1002/wat2.1150 (cited on page 1).

[7] Cook, Benjamin; Shukla, Sonali; Nazarenko, Larissa & Puma, Michael. 'Irrigation as an historical climate forcing.' In: *Clim Dyn* 44 (2015), pp. 1715–1730. DOI: https://doi.org/10.1007/s00382-014-2204-7 (cited on page 1).

[8] McDermid, Sonali; Nocco, Mallika; Lawston-Parker, Patricia; Keune, Jessica; Pokhrel, Yadu; Jain, Meha; Jägermeyr, Jonas; Brocca, Luca & Massari, Christian. 'Irrigation in the Earth system'. In: *Nature Reviews Earth & Environment* 4 (2023), pp. 435–453. DOI: 10.1038/s43017-023-00438-5 (cited on page 1).

[9] Puy, Arnald; Sheikholeslami, Razi; Gupta, Hoshin; Hall, Jim; Lankford, Bruce; Lo Piano, Samuele; Meier, Jonas; Pappenberger, Florian; Porporato, Amilcare; Vico, Giulia & Saltelli, Andrea. 'The delusive accuracy of global irrigation water withdrawal estimates'. In: *Nature Communications* 13 (Dec. 2022). DOI: 10.1038/s41467-022-30731-8 (cited on pages 1, 2).

[10] Massari, Christian; Modanesi, Sara; Dari, Jacopo; Gruber, Alexander; De Lannoy, Gabrielle J. M.; Girotto, Manuela; Quintana-Seguí, Pere; Le Page, Michel; Jarlan, Lionel; Zribi, Mehrez; Ouaadi, Nadia; Vreugdenhil, Mariëtte; Zappa, Luca; Dorigo, Wouter; Wagner, Wolfgang; Brombacher, Joost; Pelgrum, Henk; Jaquot, Pauline; Freeman, Vahid; Volden, Espen; Fernandez Prieto, Diego; Tarpanelli, Angelica; Barbetta, Silvia & Brocca, Luca. 'A Review of Irrigation Information Retrievals from Space and Their Utility for Users'. In: *Remote Sensing* 13.20 (2021). DOI: 10.3390/rs13204112 (cited on pages 1, 3).

[11] FAO. *AQUASTAT - FAO's Global Information System on Water and Agriculture*. 2021. URL: https://www.fao.org/aquastat/en/%20%5BAccessed:%20(04.11.2024,%2015:04)%5D (cited on page 1).

[12] Olivera-Guerra, Luis-Enrique; Laluet, Pierre; Altés, Víctor; Ollivier, Chloé; Pageot, Yann; Paolini, Giovanni; Chavanon, Eric; Rivalland, Vincent; Boulet, Gilles; Villar, Josep-Maria & Merlin, Olivier. 'Modeling actual water use under different irrigation regimes at district scale: Application to the FAO-56 dual crop coefficient method'. In: *Agricultural Water Management* 278 (2023), p. 108119. DOI: https://doi.org/10.1016/j.agwat.2022.108119 (cited on page 2).

[13] Elachi, Charles & Zyl, Jakob J. van. *Introduction to the physics and techniques of remote sensing*. 3rd ed. Wiley Series in Remote Sensing and Image Processing. Hoboken, New Jersey: John Wiley & Sons, Incorporated, 2021 (cited on pages 2, 3, 9).

[14] Demtröder, Wolfgang. *Experimentalphysik 2. Elektrizität und Optik*. 7th ed. Springer Spektrum, 2017, p. 204 (cited on page 2).

Die approbierte gedruckte Originalversion dieser Diplomarbeit ist an der TU Wien Bibliothek verfügbar
The approved original version of this thesis is available in print at TU Wien Bibliothek.
TU Bibliothek Your knowledge hub WIEN

[15] Schmugge, Thomas. 'Remote sensing applications in hydrology'. In: *Reviews of Geophysics* 25.2 (1987), pp. 148–152. DOI: 10.1029/RG025i002p00148 (cited on page 2).

[16] Lusch, David P. *Introduction To Microwave Remote Sensing*. Basic Science and Remote Sensing Initiative Department of Geography Michigan State University, 1999 (cited on pages 2, 3).

[17] Das, Kousik & Paul, Prabir Kumar. 'Present status of soil moisture estimation by microwave remote sensing'. In: *Cogent Geoscience* 1.1 (2015). Ed. by Dobesova, Zdena, p. 1084669. DOI: 10.1080/23312041.2015.1084669 (cited on page 2).

[18] Dorigo, Wouter; Wagner, Wolfgang; Albergel, Clement; Albrecht, Franziska; Balsamo, Gianpaolo; Brocca, Luca; Chung, Daniel; Ertl, Martin; Forkel, Matthias; Gruber, Alexander; Haas, Eva; Hamer, Paul D.; Hirschi, Martin; Ikonen, Jaakko; de Jeu, Richard; Kidd, Richard; Lahoz, William; Liu, Yi Y.; Miralles, Diego; Mistelbauer, Thomas; Nicolai-Shaw, Nadine; Parinussa, Robert; Pratola, Chiara; Reimer, Christoph; van der Schalie, Robin; Seneviratne, Sonia I.; Smolander, Tuomo & Lecomte, Pascal. 'ESA CCI Soil Moisture for improved Earth system understanding: State-of-the art and future directions'. In: *Remote Sensing of Environment* 203 (2017). Earth Observation of Essential Climate Variables, pp. 185–215. DOI: https://doi.org/10.1016/j.rse.2017.07.001 (cited on pages 3, 9).

[19] De Lannoy, Gabriëlle J. M.; Bechtold, Michel; Albergel, Clément; Brocca, Luca; Calvet, Jean-Christophe; Carrassi, Alberto; Crow, Wade T.; Rosnay, Patricia de; Durand, Michael; Forman, Barton; Geppert, Gernot; Girotto, Manuela; Hendricks Franssen, Harrie-Jan; Jonas, Tobias; Kumar, Sujay; Lievens, Hans; Lu, Yang; Massari, Christian; Pauwels, Valentijn R. N.; Reichle, Rolf H. & Steele-Dunne, Susan. 'Perspective on satellite-based land data assimilation to estimate water cycle components in an era of advanced data availability and model sophistication'. In: *Frontiers in Water* 4 (2022). DOI: 10.3389/frwa.2022.981745 (cited on page 3).

[20] Kumar, S. V.; Peters-Lidard, C. D.; Santanello, J. A.; Reichle, R. H.; Draper, C. S.; Koster, R. D.; Nearing, G. & Jasinski, M. F. 'Evaluating the utility of satellite soil moisture retrievals over irrigated areas and the ability of land data assimilation methods to correct for unmodeled processes'. In: *Hydrology and Earth System Sciences* 19.11 (2015), pp. 4463–4478. DOI: 10.5194/hess-19-4463-2015 (cited on pages 3, 4, 16).

[21] Modanesi, S.; Massari, C.; Bechtold, M.; Lievens, H.; Tarpanelli, A.; Brocca, L.; Zappa, L. & De Lannoy, G. J. M. 'Challenges and benefits of quantifying irrigation through the assimilation of Sentinel-1 backscatter observations into Noah-MP'. In: *Hydrology and Earth System Sciences* 26.18 (2022), pp. 4685–4706. DOI: 10.5194/hess-26-4685-2022 (cited on pages 3, 42).

[22] van Eekelen, M.W.; Bastiaanssen, W.G.M.; Jarmain, C.; Jackson, B.; Ferreira, F.; van der Zaag, P.; Saraiva Okello, A.; Bosch, J.; Dye, P.; Bastidas-Obando, E.; Dost, R.J.J. & Luxemburg, W.M.J. 'A novel approach to estimate direct and indirect water withdrawals from satellite measurements: A case study from the Incomati basin'. In: *Agriculture, Ecosystems & Environment* 200 (2015), pp. 126–142. DOI: https://doi.org/10.1016/j.agee.2014.10.023 (cited on page 3).

[23] Brombacher, Joost; Rezende de Oliveira Silva, Isadora; Degen, Jelle & Pelgrum, Henk. 'A novel evapotranspiration based irrigation quantification method using the hydrological similar pixels algorithm'. In: *Agricultural Water Management* 267 (2022), p. 107602. DOI: 10.1016/j.agwat.2022.107602 (cited on page 3).

[24] Olivera-Guerra, Luis; Merlin, Olivier & Er-Raki, Salah. 'Irrigation retrieval from Landsat optical/thermal data integrated into a crop water balance model: A case study over winter wheat fields in a semi-arid region'. In: *Remote Sensing of Environment* 239 (2020), p. 111627. DOI: https://doi.org/10.1016/j.rse.2019.111627 (cited on page 3).

[25] Zaussinger, F.; Dorigo, W.; Gruber, A.; Tarpanelli, A.; Filippucci, P. & Brocca, L. 'Estimating irrigation water use over the contiguous United States by combining satellite and reanalysis soil moisture data'. In: *Hydrology and Earth System Sciences* 23.2 (2019), pp. 897–923. DOI: 10.5194/hess-23-897-2019 (cited on pages 3, 4, 15, 18, 19, 42, 45).

[26] Zappa, Luca; Schlaffer, Stefan; Bauer-Marschallinger, Bernhard; Nendel, Claas; Zimmerman, Beate & Dorigo, Wouter. 'Detection and Quantification of Irrigation Water Amounts at 500 m Using Sentinel-1 Surface Soil Moisture'. In: *Remote Sensing* 13.9 (2021). DOI: 10.3390/rs13091727 (cited on pages 3, 4, 18, 42, 43).

Die approbierte gedruckte Originalversion dieser Diplomarbeit ist an der TU Wien Bibliothek verfügbar
The approved original version of this thesis is available in print at TU Wien Bibliothek.
TU Bibliothek Your knowledge hub WIEN

[27] Zappa, Luca; Schlaffer, Stefan; Brocca, Luca; Vreugdenhil, Mariette; Nendel, Claas & Dorigo, Wouter. 'How accurately can we retrieve irrigation timing and water amounts from (satellite) soil moisture?' In: *International Journal of Applied Earth Observation and Geoinformation* 113 (2022), p. 102979. DOI: https://doi.org/10.1016/j.jag.2022.102979 (cited on pages 3, 5, 17, 18, 42).

[28] Zappa, Luca; Dari, Jacopo; Modanesi, Sara; Quast, Raphael; Brocca, Luca; De Lannoy, Gabrielle; Massari, Christian; Quintana-Seguí, Pere; Barella-Ortiz, Anais & Dorigo, Wouter. 'Benefits and pitfalls of irrigation timing and water amounts derived from satellite soil moisture'. In: *Agricultural Water Management* 295 (2024), p. 108773. DOI: https://doi.org/10.1016/j.agwat.2024.108773 (cited on pages 3, 5, 18, 42, 43).

[29] Brocca, Luca; Massari, Christian; Ciabatta, Luca; Moramarco, Tommaso; Penna, Daniele; Zuecco, Giulia; Pianezzola, Luisa; Borga, Marco; Matgen, Patrick & Martínez-Fernández, José. 'Rainfall estimation from in situ soil moisture observations at several sites in Europe: an evaluation of the SM2RAIN algorithm'. In: *Journal of Hydrology and Hydromechanics* 63.3 (2015), pp. 201–209. DOI: doi:10.1515/johh-2015-0016 (cited on pages 3, 4, 11, 42, 43).

[30] Dari, J.; Brocca, L.; Modanesi, S.; Massari, C.; Tarpanelli, A.; Barbetta, S.; Quast, R.; Vreugdenhil, M.; Freeman, V.; Barella-Ortiz, A.; Quintana-Seguí, P.; Bretreger, D. & Volden, E. 'Regional data sets of high-resolution (1 and 6 km) irrigation estimates from space'. In: *Earth System Science Data* 15.4 (2023), pp. 1555–1575. DOI: 10.5194/essd-15-1555-2023 (cited on pages 3, 4, 7, 13, 42, 43).

[31] Dari, Jacopo; Quintana-Seguí, Pere; Morbidelli, Renato; Saltalippi, Carla; Flammini, Alessia; Giugliarelli, Elena; Escorihuela, María José; Stefan, Vivien & Brocca, Luca. 'Irrigation estimates from space: Implementation of different approaches to model the evapotranspiration contribution within a soil-moisture-based inversion algorithm'. In: *Agricultural Water Management* 265 (2022), p. 107537. DOI: https://doi.org/10.1016/j.agwat.2022.107537 (cited on pages 3, 4, 42, 43).

[32] Dari, Jacopo; Brocca, Luca; Quintana-Seguí, Pere; Escorihuela, María José; Stefan, Vivien & Morbidelli, Renato. 'Exploiting High-Resolution Remote Sensing Soil Moisture to Estimate Irrigation Water Amounts over a Mediterranean Region'. In: *Remote Sensing* 12.16 (2020). DOI: 10.3390/rs12162593 (cited on pages 3, 4, 7, 12, 42, 43).

[33] Jalilvand, Ehsan; Tajrishy, Masoud; Ghazi Zadeh Hashemi, Sedigheh Alsadat & Brocca, Luca. 'Quantification of irrigation water using remote sensing of soil moisture in a semi-arid region'. In: *Remote Sensing of Environment* 231 (2019), p. 111226. DOI: 10.1016/j.rse.2019.111226 (cited on pages 3, 4).

[34] Zohaib, Muhammad & Choi, Minha. 'Satellite-based global-scale irrigation water use and its contemporary trends'. In: *Science of The Total Environment* 714 (Jan. 2020), p. 136719. DOI: 10.1016/j.scitotenv.2020.136719 (cited on pages 4, 11, 16–18, 41, 42).

[35] Quast, Raphael; Albergel, Clément; Calvet, Jean-Christophe & Wagner, Wolfgang. 'A Generic First-Order Radiative Transfer Modelling Approach for the Inversion of Soil and Vegetation Parameters from Scatterometer Observations'. In: *Remote Sensing* 11.3 (2019). DOI: 10.3390/rs11030285 (cited on page 4).

[36] Beck, Hylke; Zimmermann, Niklaus; McVicar, Tim R.; Vergopolan, Noemi; Berg, Alexis & Wood, Eric. 'Present and future Köppen-Geiger climate classification maps at 1-km resolution'. In: *Scientific Data* 5 (2018). DOI: https://doi.org/10.1038/sdata.2018.214 (cited on page 7).

[37] Bovolo, C. I.; Blenkinsop, S.; Majone, B.; Zambrano-Bigiarini, M.; Fowler, H. J.; Bellin, A.; Burton, A.; Barceló, D.; Grathwohl, P. & Barth, J. A. C. 'Climate Change, Water Resources and Pollution in the Ebro Basin: Towards an Integrated Approach'. In: *The Ebro River Basin*. Ed. by Barceló, Damià & Petrovic, Mira. Berlin, Heidelberg: Springer Berlin Heidelberg, 2011, pp. 295–329. DOI: 10.1007/698_2010_86 (cited on page 7).

[38] Laluet, Pierre; Olivera-Guerra, Luis Enrique; Altés, Víctor; Paolini, Giovanni; Ouaadi, Nadia; Rivalland, Vincent; Jarlan, Lionel; Villar, Josep Maria & Merlin, Olivier. 'Retrieving the irrigation actually applied at district scale: Assimilating high-resolution Sentinel-1-derived soil moisture data into a FAO-56-based model'. In: *Agricultural Water Management* 293 (2024), p. 108704. DOI: https://doi.org/10.1016/j.agwat.2024.108704 (cited on page 7).

Die approbierte gedruckte Originalversion dieser Diplomarbeit ist an der TU Wien Bibliothek verfügbar
The approved original version of this thesis is available in print at TU Wien Bibliothek.
TU Bibliothek Your knowledge hub WIEN

[39] Murray-Darling Basin Authority. *Climate and river health*. 2023. URL: https://www.mdba.gov.au/climate-and-river-health/climate,%20(last%20access:19.12.2024,14:34) (cited on page 7).

[40] Bretreger, David; Yeo, In-Young; Hancock, Greg & Willgoose, Garry. 'Monitoring irrigation using landsat observations and climate data over regional scales in the Murray-Darling Basin'. In: *Journal of Hydrology* 590.125356 (2020). DOI: 10.1016/j.jhydrol.2020.125356 (cited on pages 8, 41).

[41] Dorigo, Wouter; Preimesberger, Wolfgang; Stradiotti, Pietro; Kidd, Richard; Schalie, Robin van der; Vliet, Mendy van der; Rodriguez-Fernandez, Nemesio; Madelon, Remi & Baghdadi, Nicolas. *ESA Climate Change Initiative Plus - Soil Moisture Algorithm Theoretical Baseline Document (ATBD) Supporting Product Version 08.1*. Version version 1.1. Sept. 2023. DOI: 10.5281/zenodo.8320869. URL: https://doi.org/10.5281/zenodo.8320869 (cited on pages 9, 10).

[42] Rodell, M.; Houser, P. R.; Jambor, U.; Gottschalck, J.; Mitchell, K.; Meng, C.-J.; Arsenault, K.; Cosgrove, B.; Radakovich, J.; Bosilovich, M.; Entin, J. K.; Walker, J. P.; Lohmann, D. & Toll, D. 'The Global Land Data Assimilation System'. In: *Bulletin of the American Meteorological Society* 85.3 (2004), pp. 381–394. DOI: 10.1175/BAMS-85-3-381 (cited on pages 9, 10).

[43] Dorigo, Wouter; Stradiotti, Pietro; Preimesberger, Wolfgang; Kidd, Richard; Schalie, Robin van der; Frederikse, Thomas; Rodriguez-Fernandez, Nemesio & Baghdadi, Nicolas. *ESA Climate Change Initiative Plus - Soil Moisture Algorithm Theoretical Baseline Document (ATBD) Supporting Product Version 09.0*. Sept. 2024. DOI: 10.5281/zenodo.13860922. URL: https://doi.org/10.5281/zenodo.13860922 (cited on pages 9, 10).

[44] Gruber, A.; Su, C.-H.; Zwieback, S.; Crow, W.; Dorigo, W. & Wagner, W. 'Recent advances in (soil moisture) triple collocation analysis'. In: *International Journal of Applied Earth Observation and Geoinformation* 45 (2016). Advances in the Validation and Application of Remotely Sensed Soil Moisture - Part 1, pp. 200–211. DOI: https://doi.org/10.1016/j.jag.2015.09.002 (cited on page 9).

[45] Gruber, A.; Scanlon, T.; Schalie, R. van der; Wagner, W. & Dorigo, W. 'Evolution of the ESA CCI Soil Moisture climate data records and their underlying merging methodology'. In: *Earth System Science Data* 11.2 (2019), pp. 717–739. DOI: 10.5194/essd-11-717-2019 (cited on page 9).

[46] Wagner, Wolfgang; Lemoine, Guido & Rott, Helmut. 'A Method for Estimating Soil Moisture from ERS Scatterometer and Soil Data'. In: *Remote Sensing of Environment* 70.2 (1999), pp. 191–207. DOI: https://doi.org/10.1016/S0034-4257(99)00036-X (cited on page 10).

[47] Naeimi, Vahid; Scipal, Klaus; Bartalis, Zoltan; Hasenauer, Stefan & Wagner, Wolfgang. 'An Improved Soil Moisture Retrieval Algorithm for ERS and METOP Scatterometer Observations'. In: *IEEE Transactions on Geoscience and Remote Sensing* 47.7 (2009), pp. 1999–2013. DOI: 10.1109/TGRS.2008.2011617 (cited on page 10).

[48] Owe, Manfred; Jeu, Richard de & Holmes, Thomas. 'Multisensor historical climatology of satellite-derived global land surface moisture'. In: *Journal of Geophysical Research: Earth Surface* 113.1 (2008). Cited by: 847; All Open Access, Green Open Access. DOI: 10.1029/2007JF000769 (cited on page 10).

[49] Dorigo, W.; Preimesberger, W.; Hahn, S.; Van der Schalie, R.; De Jeu, R.; Kidd, R.; Rodriguez-Fernandez, N.; Hirschi, M.; Stradiotti, P.; Frederikse, T.; Gruber, A. & Madelon, R. 'ESA Soil Moisture Climate Change Initiative (Soil Moisture cci): ACTIVE product, Version 08.1'. In: *NERC EDS Centre for Environmental Data Analysis* (2023) (cited on page 10).

[50] Dorigo, W.; Preimesberger, W.; Hahn, S.; Van der Schalie, R.; De Jeu, R.; Kidd, R.; Rodriguez-Fernandez, N.; Hirschi, M.; Stradiotti, P.; Frederikse, T.; Gruber, A. & Madelon, R. 'ESA Soil Moisture Climate Change Initiative (Soil Moisture cci): PASSIVE product, Version 08.1'. In: *NERC EDS Centre for Environmental Data Analysis* (2023) (cited on page 10).

[51] Dorigo, Wouter; Preimesberger, Wolfgang; Hahn, Sebastian; Van der Schalie, Robin; De Jeu, R.; Kidd, Richard; Rodriguez-Fernandez, Nemesio; Hirschi, M.; Stradiotti, Pietro; Frederikse, Thomas; Gruber, Alexander & Duchemin, D. 'ESA Soil Moisture Climate Change Initiative (Soil Moisture cci): COMBINED product'. Version version 09.1. In: *NERC EDS Centre for Environmental Data Analysis* (2024). DOI: 10.5285/0e346e1e1e164ac99c60098848537a29 (cited on page 11).

Die approbierte gedruckte Originalversion dieser Diplomarbeit ist an der TU Wien Bibliothek verfügbar
The approved original version of this thesis is available in print at TU Wien Bibliothek.
TU Bibliothek Your knowledge hub WIEN

[52] Kerr, Yann H.; Waldteufel, Philippe; Wigneron, Jean-Pierre; Martinuzzi, Jean-Michel; Font, Jordi & Berger, Michael. 'Soil moisture retrieval from space: The Soil Moisture and Ocean Salinity (SMOS) mission'. In: *IEEE Transactions on Geoscience and Remote Sensing* 39.8 (2001). Cited by: 1406, pp. 1729–1735. DOI: 10.1109/36.942551 (cited on page 11).

[53] Kerr, Y.H.; Al-Yaari, A.; Rodriguez-Fernandez, N.; Parrens, M.; Molero, B.; Leroux, D.; Bircher, S.; Mahmoodi, A.; Mialon, A.; Richaume, P.; Delwart, S.; Al Bitar, A.; Pellarin, T.; Bindlish, R.; Jackson, T.J.; Rüdiger, C.; Waldteufel, P.; Mecklenburg, S. & Wigneron, J.-P. 'Overview of SMOS performance in terms of global soil moisture monitoring after six years in operation'. In: *Remote Sensing of Environment* 180 (2016). Special Issue: ESA's Soil Moisture and Ocean Salinity Mission - Achievements and Applications, pp. 40–63. DOI: https://doi.org/10.1016/j.rse.2016.02.042 (cited on page 11).

[54] Entekhabi, Dara; Njoku, Eni G.; O'Neill, Peggy E.; Kellogg, Kent H.; Crow, Wade T.; Edelstein, Wendy N.; Entin, Jared K.; Goodman, Shawn D.; Jackson, Thomas J.; Johnson, Joel; Kimball, John; Piepmeier, Jeffrey R.; Koster, Randal D.; Martin, Neil; McDonald, Kyle C.; Moghaddam, Mahta; Moran, Susan; Reichle, Rolf; Shi, J. C.; Spencer, Michael W.; Thurman, Samuel W.; Tsang, Leung & Van Zyl, Jakob. 'The Soil Moisture Active Passive (SMAP) Mission'. In: *Proceedings of the IEEE* 98.5 (2010), pp. 704–716. DOI: 10.1109/JPROC.2010.2043918 (cited on page 11).

[55] Muñoz-Sabater, J. 'ERA5-Land hourly data from 1950 to present'. In: *Copernicus Climate Change Service (C3S) Climate Data Store (CDS)* (2019). DOI: 10.24381/cds.e2161bac (cited on pages 11, 15).

[56] Muñoz-Sabater, J.; Dutra, E.; Agustí-Panareda, A.; Albergel, C.; Arduini, G.; Balsamo, G.; Boussetta, S.; Choulga, M.; Harrigan, S.; Hersbach, H.; Martens, B.; Miralles, D. G.; Piles, M.; Rodríguez-Fernández, N. J.; Zsoter, E.; Buontempo, C. & Thépaut, J.-N. 'ERA5-Land: a state-of-the-art global reanalysis dataset for land applications'. In: *Earth System Science Data* 13.9 (2021), pp. 4349–4383. DOI: 10.5194/essd-13-4349-2021 (cited on page 11).

[57] SAIH. *Sistema automatico de Informacion Hidrologica del Ebro*. URL: https://www.saihebro.com/tiempo-real/mapa-riegos-CG-toda-la-cuenca(Accessed:(28.11.2024,16:42)) (cited on page 12).

[58] Jansen, Louisa & Di Gregorio, Antonio. *Land Cover Classification System (LCCS): Classification Concepts and User Manual*. Jan. 2000 (cited on page 13).

[59] Bezy, Jean-Loup; Gourmelon, Georges; Bessudo, Richard; Baudin, Gilles; Sontag, Heinz & Weiss, Stefan. *Medium resolution imaging spectrometer (MERIS)*. Feb. 1999. DOI: 10.1109/IGARSS.1999.774655 (cited on page 13).

[60] Defourny, P.; Lamarche, C.; Bontemps, S.; T., De Maet; Van Bogaert, E.; I., Moreau; Brockmann, C.; Boettcher, M.; Kirches, G.; Wevers, J. & Santoro, M. *CCI Land Cover Product User Guide v2*. Tech. rep. ESA, 2017 (cited on page 13).

[61] Hirschi, M.; Stradiotti, P.; Preimesberger, W.; Dorigo, W. & Kidd, R. 'ESA Climate Change Initiative Plus - Soil Moisture Product Validation and Intercomparison Report (PVIR) Supporting Product version v08.1 (issue 1.0)'. In: *Zenodo* (2023). DOI: 10.5281/zenodo.8320930 (cited on page 15).

[62] Escorihuela, Maria Jose & Quintana-Seguí, Pere. 'Comparison of remote sensing and simulated soil moisture datasets in Mediterranean landscapes'. In: *Remote Sensing of Environment* 180 (2016). Special Issue: ESA's Soil Moisture and Ocean Salinity Mission - Achievements and Applications, pp. 99–114. DOI: https://doi.org/10.1016/j.rse.2016.02.046 (cited on pages 15, 16, 21).

[63] Brocca, L.; Hasenauer, S.; Lacava, T.; Melone, F.; Moramarco, T.; Wagner, W.; Dorigo, W.; Matgen, P.; Martínez-Fernández, J.; Llorens, P.; Latron, J.; Martin, C. & Bittelli, M. 'Soil moisture estimation through ASCAT and AMSR-E sensors: An intercomparison and validation study across Europe'. In: *Remote Sensing of Environment* 115.12 (2011), pp. 3390–3408. DOI: https://doi.org/10.1016/j.rse.2011.08.003 (cited on page 16).

[64] Nair, Akhilesh S. & Indu, J. 'Improvement of land surface model simulations over India via data assimilation of satellite-based soil moisture products'. In: *Journal of Hydrology* 573 (2019), pp. 406–421. DOI: https://doi.org/10.1016/j.jhydrol.2019.03.088 (cited on page 16).

Die approbierte gedruckte Originalversion dieser Diplomarbeit ist an der TU Wien Bibliothek verfügbar
The approved original version of this thesis is available in print at TU Wien Bibliothek.
TU Bibliothek Your knowledge hub WIEN

[65] Lawston, Patricia M.; Santanello Jr, Joseph A. & Kumar, Sujay V. 'Irrigation Signals Detected From SMAP Soil Moisture Retrievals'. In: *Geophysical Research Letters* 44.23 (2017), pp. 11, 860–11, 867. DOI: https://doi.org/10.1002/2017GL075733 (cited on page 18).

[66] Dorigo, W. A.; Scipal, K.; Parinussa, R. M.; Liu, Y. Y.; Wagner, W.; Jeu, R. A. M. de & Naeimi, V. 'Error characterisation of global active and passive microwave soil moisture datasets'. In: *Hydrology and Earth System Sciences* 14.12 (2010), pp. 2605–2616. DOI: 10.5194/hess-14-2605-2010 (cited on page 19).

[67] Brocca, Luca; Melone, F.; Moramarco, T.; Wagner, Wolfgang & Albergel, Clement. 'Scaling and Filtering Approaches for the Use of Satellite Soil Moisture Observations'. In: CRC Press, Oct. 2013, pp. 411–426. DOI: 10.1201/b15610-21 (cited on page 21).

[68] Kragh, S. J.; Dari, J.; Modanesi, S.; Massari, C.; Brocca, L.; Fensholt, R.; Stisen, S. & Koch, J. 'An intercomparison of approaches and frameworks to quantify irrigation from satellite data'. In: *Hydrology and Earth System Sciences* 28.3 (2024), pp. 441–457. DOI: 10.5194/hess-28-441-2024 (cited on page 43).

[69] '2018 Irrigation and Water Management Survey'. In: *United States Department of Agriculture* 3 (2019) (cited on page 43).

Die approbierte gedruckte Originalversion dieser Diplomarbeit ist an der TU Wien Bibliothek verfügbar
The approved original version of this thesis is available in print at TU Wien Bibliothek.
TU Bibliothek Your knowledge hub WIEN

List of Figures

Die approbierte gedruckte Originalversion dieser Diplomarbeit ist an der TU Wien Bibliothek verfügbar
The approved original version of this thesis is available in print at TU Wien Bibliothek.
TU Wien Bibliothek Your knowledge hub

Die approbierte gedruckte Originalversion dieser Diplomarbeit ist an der TU Wien Bibliothek verfügbar
The approved original version of this thesis is available in print at TU Wien Bibliothek.
TU Bibliothek Your knowledge hub WIEN

List of Tables

Die approbierte gedruckte Originalversion dieser Diplomarbeit ist an der TU Wien Bibliothek verfügbar
The approved original version of this thesis is available in print at TU Wien Bibliothek.